Decentralized Feedback Controllers for Robust Stabilization of Periodic Orbits of Hybrid Systems: Application to Bipedal Walking

Kaveh Akbari Hamed, *Member, IEEE,* and Robert D. Gregg, *Senior Member, IEEE*

Abstract—This paper presents a systematic algorithm to design time-invariant decentralized feedback controllers to exponentially and robustly stabilize periodic orbits for hybrid dynamical systems against possible uncertainties in discrete-time phases. The algorithm assumes a family of parameterized and decentralized nonlinear controllers to coordinate interconnected hybrid subsystems based on a common phasing variable. The exponential and $\mathcal{H}_2$ robust stabilization problems of periodic orbits are translated into an iterative sequence of optimization problems involving bilinear and linear matrix inequalities. By investigating the properties of the Poincaré map, some sufficient conditions for the convergence of the iterative algorithm are presented. The power of the algorithm is finally demonstrated through designing a set of robust stabilizing local nonlinear controllers for walking of an underactuated 3D autonomous bipedal robot with 9 degrees of freedom, impact model uncertainties, and a decentralization scheme motivated by amputee locomotion with a transpelvic prosthetic leg.

Index Terms—Decentralized Nonlinear Control, Hybrid Periodic Orbits, Underactuated 3D Bipedal Robots.

I. Introduction

THE objective of this paper is to present a systematic algorithm, based on an iterative sequence of optimization problems, to design time-invariant *decentralized* feedback controllers to exponentially and robustly stabilize periodic orbits for hybrid dynamical systems. The algorithm assumes a parameterized family of local nonlinear controllers which provides cooperation among interconnected subsystems in the presence of uncertain discrete-time phases. It can provably stabilize walking gaits of underactuated 3D bipedal robots composed of interconnected subsystems with impact model uncertainties.

Previous work on robotic walking made use of multi-level *centralized* nonlinear feedback control architectures to stabilize periodic orbits [1]–[22]. One drawback of employing centralized controllers is that these controllers *cannot* be

easily transferred to powered prosthetic legs, which act as decentralized subsystems. Furthermore, a substantial body of research in neurophysiology suggests that there is a great deal of hierarchical structure and locality of control in both insect and mammalian walking [23]. Although powered prosthetic legs already use decentralized feedback controllers based on tracking reference joint torques [24], kinematics [25], or impedances [26] to resemble human behavior, these *time-varying* and *linear* control methods require different control parameters at different time periods to handle the nonlinear dynamics of the gait cycle. The resulting "finite state machine" requires clinicians to spend significant amounts of time tuning each controller to a patient [27] and risks instability when perturbations cause the wrong controller to be used at the wrong time [28]–[30]. The limitations of this sequential control method could possibly be addressed by the unifying *nonlinear* controllers used in dynamic walking robots, but their centralized feedback architectures would require state measurements from both the prosthesis and human body, i.e., two interconnected subsystems. These key roadblocks to cooperative human-machine walking necessitate the application of decentralized nonlinear feedback control and thereby underline the importance of having algorithms to systematically design these controllers.

While the problem of designing decentralized controllers for large-scale complex systems is well studied in the literature [31]–[33], existing results are tailored for stabilization of *equilibrium points* of ordinary differential equations (ODEs) and *not* periodic orbits of hybrid dynamical systems [34]–[37]. Significant complexity in the design of decentralized control schemes for dynamical models of legged robots arises from the high dimensionality, strong interactions among subsystems, underactuation, and hybrid nature of these models. In addition, the most basic tool for analyzing the stability of periodic orbits of hybrid dynamical systems, the Poincaré return map [2], [34], [38]–[40], unfortunately has some serious limitations. In almost all practical cases, there is *not* a close-form expression for the Poincaré map and it must be estimated *numerically*. This complicates the design of decentralized controllers for asymptotic and robust stabilization of hybrid periodic orbits.

The contribution of this paper is to present a systematic algorithm to design a class of time-invariant decentralized nonlinear feedback controllers that exponentially and robustly stabilize periodic orbits for the hybrid systems arising from bipedal robots. The proposed algorithm assumes a finite set of parameterized local controllers which are coordinated based on

a *common phasing variable*. We investigate nonlinear stability tools for hybrid systems to formulate the problem of designing decentralized nonlinear controllers as an iterative sequence of optimization problems involving Bilinear and Linear Matrix Inequalities (BMIs and LMIs). By design these optimization problems will be solved with available software packages. Some sufficient conditions for the convergence of the iterative algorithm will be presented. The key features of the proposed algorithm can be summarized as follows: (1) it addresses a general form of parameterized decentralized nonlinear controllers; (2) it deals with underactuation and impact model uncertainties; and (3) the BMI optimization problem takes into account the interactions among the cooperative subsystems while searching for the robust stabilizing decentralized controllers, preventing the need to employ impractical high-gain local controllers [28], asymptotic observers, or expensive force sensors [30] to deal with interactions.

Our previous work employed the BMI optimization framework for the systematic design of centralized nonlinear feedback controllers for bipedal robots [41]–[43] and experimentally validated the theoretical results on the underactuated 3D bipedal robot ATRIAS with point feet [44], [45]. Reference [43] also investigated the centralized $\mathcal{H}_\infty$ feedback design problem without formal mathematical proofs. The BMI algorithm of [41] for designing centralized control problems was *not* iterative, whereas we have observed that for decentralized control problems the BMI algorithm must be applied in an *iterative* manner to converge to a stabilizing solution. This underlines the importance of (1) developing iterative BMI algorithms and (2) analyzing the convergence of the iterative algorithms. Furthermore, [41] did *not* consider $\mathcal{H}_2$ feedback design problems. The current paper presents a systematic and *iterative* BMI algorithm for the design of decentralized feedback controllers. In particular, a novel class of decentralized feedback controllers is first developed and then the BMI framework is extended to the exponential and $\mathcal{H}_2$ robust stabilization problems of periodic orbits with mathematical proofs for the convergence to stabilizing solutions. Finally to demonstrate the power of the algorithm, we control the walking gait of a 3D autonomous bipedal robot with 9 degrees of freedom (DOFs) and 6 actuators. The robot's model includes a two-part decentralization scheme corresponding to a transpelvic (hip disarticulated) amputee walking with a robotic prosthetic leg. A byproduct of this work is the first known control strategy for a powered 3-DOF transpelvic prosthetic leg.

Some parts of the BMI algorithm for the exponential stabilization problem of decentralized controllers were presented in the preliminary work [46] without dealing with model uncertainties. The current paper extends the BMI algorithm to address the $\mathcal{H}_2$ robust stabilization problem against external disturbances and uncertainties in the impact model, which is known to be the most uncertain or inaccurate portion for hybrid models of walking. It also presents sufficient conditions for the proof of convergence in the extended BMI algorithm. To demonstrate the robustness, the paper numerically evaluates the biped system's performance in two simulators with different contact and impact models.

This paper is organized as follows. Section II presents

hybrid models of walking and develops the decentralized feedback control scheme. The exponential and robust stabilization problems are presented in Section III. The iterative BMI algorithm for exponential stabilization is developed in Section IV. Section V extends the BMI algorithm for the $\mathcal{H}_2$ control problem. Sufficient conditions for the convergence of the algorithm are presented in Section VI. Section VII applies the results to the hybrid models of walking and presents detailed numerical simulations. Section VIII finally presents some concluding remarks.

II. HYBRID MODEL

We consider single-phase hybrid dynamical systems arising from bipedal walking as follows

$$\Sigma : \begin{cases} \dot{x} = f(x) + g(x)\,u, & x^- \notin \mathcal{S} \\ x^+ = \Delta(x^-) + d, & x^- \in \mathcal{S}, \end{cases} \quad (1)$$

in which $x \in \mathcal{X}$ and $u \in \mathcal{U}$ denote the *global state variables* and *global continuous-time control inputs*, respectively. The *global state manifold* and the *global set of admissible control inputs* are represented by $\mathcal{X} \subset \mathbb{R}^n$ and $\mathcal{U} \subset \mathbb{R}^m$ for some positive integers n and m. The evolution of the system during the continuous-time phase is described by the ODE $\dot{x} = f(x) + g(x)\,u$, in which the drift vector field $f : \mathcal{X} \to T\mathcal{X}$ and columns of g are assumed to be smooth (i.e., $\mathcal{C}^\infty$). $T\mathcal{X}$ also denotes the tangent bundle of the state manifold $\mathcal{X}$. The discrete-time portion of the hybrid system is also represented by the instantaneous mapping $x^+ = \Delta(x^-) + d$, where $\Delta : \mathcal{X} \to \mathcal{X}$ is a $\mathcal{C}^\infty$ *reset map*, $d \in \mathcal{D}$ is an *unknown and bounded discrete-time disturbance input*, and $x^-(t) := \lim_{\tau \nearrow t} x(\tau)$ and $x^+(t) := \lim_{\tau \searrow t} x(\tau)$ denote the left and right limits of the state trajectory $x(t)$, respectively. The *set of admissible disturbance inputs* $\mathcal{D} \subset \mathbb{R}^n$ is taken as a bounded, connected and open neighborhood of the origin. The *switching manifold* $\mathcal{S}$ is then represented by

$$\mathcal{S} := \{ x \in \mathcal{X} \mid s(x) = 0,\ \sigma(x) < 0 \}, \quad (2)$$

on which the state solutions of the hybrid system undergo an abrupt change according to the re-initialization rule $x^+ = \Delta(x^-) + d$. In addition, $s : \mathcal{X} \to \mathbb{R}$ is a $\mathcal{C}^\infty$ real-valued *switching function* which satisfies $\frac{\partial s}{\partial x}(x) \neq 0$ for all $x \in \mathcal{X}$. Finally, $\sigma : \mathcal{X} \to \mathbb{R}$ is a $\mathcal{C}^\infty$ real-valued function such that $\sigma(x) < 0$ determines feasible switching events. The solutions of the hybrid system (1) are constructed by piecing together the flows of the continuous-time phase such that the re-initialization rule is applied when the flows intersect the switching manifold. For the purpose of this paper, the solutions are also assumed to be right continuous.

Remark 1: To simplify the analysis and design procedure of decentralized feedback controllers, we consider single-phase hybrid dynamical systems. Section VII will extend the analysis to hybrid models of robot walking with two continuous-time phases including the right and left leg stance phases.

A. Interconnected Hybrid Subsystems

Throughout this paper, we shall assume that the hybrid model (1) is composed of *two interconnected hybrid subsystems* Σ_1 and Σ_2 in which the *local state variables* and

local control inputs for the subsystem Σ_i are represented by $x_i \in \mathcal{X}_i$ and $u_i \in \mathcal{U}_i$, respectively. In our notation, the subscript $i \in \{1, 2\}$ denotes the subsystem number. Furthermore, $\mathcal{X}_i \subset \mathbb{R}^{n_i}$ and $\mathcal{U}_i \subset \mathbb{R}^{m_i}$ are the *local state manifold* and *local admissible set of control inputs* for some positive integers n_i and m_i such that $n_1 + n_2 = n$ and $m_1 + m_2 = m$. Our motivation comes from biomimetic control of powered prostheses for which the typical model may consist of two interconnected subsystems including the "human" body and "prosthetic" part (see Fig. 1). Without loss of generality, we assume that the global state variables and global control inputs can be decomposed as $x = (x_1^\top, x_2^\top)^\top$ and $u = (u_1^\top, u_2^\top)^\top$ which result in $\mathcal{X} = \mathcal{X}_1 \times \mathcal{X}_2$ and $\mathcal{U} = \mathcal{U}_1 \times \mathcal{U}_2$. In our notation, "$\top$" denotes the matrix transpose.

Remark 2: Although the analysis and design procedure of local controllers are presented for hybrid systems comprising two interconnected subsystems, the results can be extended to systems comprising multiple subsystems, including decentralized control of multi-legged robots.

B. Transversal Period-One Orbit

Throughout this paper, we shall assume that there is a period-one orbit $\mathcal{O}$ for the hybrid model (1) *in the absence* of the external disturbance input (i.e., $d = 0$), and this orbit is transversal to the switching manifold $\mathcal{S}$. This becomes more clear in the following assumption.

Assumption 1 (Transversal Period-One Orbit): There exist a bounded period $T^\star > 0$ (referred to as the *fundamental period*), *nominal smooth local control inputs* $u_i^\star : [0, T^\star] \to \mathcal{U}_i$ for $i \in \{1, 2\}$, and a *nominal smooth global state solution* $\varphi^\star : [0, T^\star] \to \mathcal{X}$ such that (1) the continuous-time phase ODE is satisfied, i.e.,

$$\dot{\varphi}^\star(t) = f(\varphi^\star(t)) + g(\varphi^\star(t)) u^\star(t), \quad 0 \le t \le T^\star \quad (3)$$

$$\varphi^\star(t) \notin \mathcal{S}, \quad 0 \le t < T^\star \quad \text{and} \quad \varphi^\star(T^\star) \in \mathcal{S}, \quad (4)$$

where $u^\star(t) := (u_1^{\star\top}(t), u_2^{\star\top}(t))^\top$, (2) the *periodicity condition* is met in the absence of the external disturbance input d, that is, $\varphi^\star(0) = \Delta(\varphi^\star(T^\star))$, and (3) the *transversality condition* holds, i.e., $\dot{s}(T^\star) := \frac{\partial s}{\partial x}(\varphi^\star(T^\star)) \dot{\varphi}^\star(T^\star) \neq 0$. Then,

$$\mathcal{O} := \{x = \varphi^\star(t) \mid 0 \le t < T^\star\} \quad (5)$$

is a *period-one orbit* for the hybrid model (1) corresponding to $d = 0$. Furthermore, according to the construction procedure,

$$\{x^\star\} := \overline{\mathcal{O}} \cap \mathcal{S} = \{\varphi^\star(T^\star)\} \quad (6)$$

is a singleton, in which $\overline{\mathcal{O}}$ denotes the set closure of $\mathcal{O}$.

C. Class of Decentralized Feedback Controllers

The objective of this section is to present the proposed decentralized feedback control structure to stabilize the periodic orbit $\mathcal{O}$ for the hybrid model (1). In our proposed structure, the local feedback controllers are *parameterized* and *general nonlinear feedback laws* which have access to their own local measurements (i.e., local state variables x_i) as well as a *subset* of measurable global variables. *Global variables* are defined as quantities which are dependent on the global state variables.
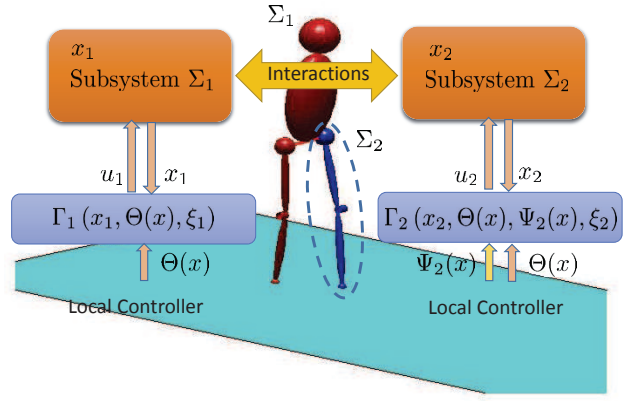

Fig. 1: Illustration of the local subsystems and proposed decentralized feedback control scheme for stabilization of periodic orbits for bipedal walking. The subsystem Σ_2 (i.e., prosthetic part), shown by the dashed ellipse, includes the degrees of freedom and actuators for the left leg. Σ_1 (i.e., human part) consists of the rest of the model.

The global variable $\pi(x) = \pi(x_1, x_2)$ is said to be *measurable* for the subsystem Σ_i if there are sensors to measure it along the solutions of the subsystem Σ_i. For the purpose of this paper, we make the following assumption.

Assumption 2 (Measurable Global Variables): The set of measurable global variables for the subsystem Σ_i, $i \in \{1, 2\}$, can be written in the following chain form

$$\Psi_i(x) := \left(\psi_i^\top(x), \dot{\psi}_i^\top(x), \cdots, \psi_i^{(r-1)\top}(x) \right)^\top \in \mathbb{R}^{rv_i}, \quad (7)$$

for some smooth measurable global variables $\psi_i(x) \in \mathbb{R}^{v_i}$ and some positive integers $v_i \ge 1$ and $r \ge 1$. We further assume that the control input u does *not* explicitly appear in the equations of $\psi_i(x)$, $\dot{\psi}_i(x)$, $\cdots$, and $\psi_i^{(r-1)}(x) := \frac{\mathrm{d}^{r-1}}{\mathrm{d}t^{r-1}} \psi_i(x)$.

Example 1: In this paper, we study the available measurable global variables for the case of a transpelvic amputee and hip-knee powered prosthesis shown in Fig. 1. Without loss of generality we assume that subsystems Σ_1 and Σ_2 represent the human and prosthetic leg parts, respectively. We further suppose that the local state variables x_1 include the global orientation of the human part with respect to the world frame (assumed to come from the vestibular system), whereas the local state variables x_2 only include the shape variables for the prosthetic part. We therefore must utilize inertial measurement units (IMUs) for measurement of orientation in the prosthetic leg controller. Since the global orientation is implicitly included in local state variables x_1, the set of external measurable global variables for the subsystem Σ_1 can be chosen as empty, i.e., $\Psi_1(x) = \emptyset$. However, we assume that the prosthetic orientation measurements come from two IMUs attached to the thigh links: one on the human thigh and the other on the prosthetic thigh. The set of measurable global variables $\Psi_2(x)$ for Σ_2 can then be chosen as the Euler angles in $\psi_2(x)$ and their first-order time-derivatives $\dot{\psi}_2(x)$ provided by these IMUs, i.e., $\Psi_2(x) = (\psi_2^\top(x), \dot{\psi}_2^\top(x))^\top$. Here r is taken as 2 due to the second-order nature of the

dynamics. This example will be clarified with more details and numerical simulations in Section VII. The use of two IMUs by the prosthesis will allow the BMI optimization algorithm to more easily find robust stabilizing decentralized feedback controllers in Section VII-B. There is precedence for wearing sensors on the sound leg in prosthetic control methods [47], [48].

In order to coordinate the action of local controllers in the proposed structure, we then make use of a *common phasing variable* that is measurable for both subsystems Σ_1 and Σ_2. The *phasing variable* is a smooth and scalar global variable which is strictly monotonic (i.e., strictly increasing or decreasing) along the desired periodic orbit $\mathcal{O}$. We make this idea more clear in the following assumption.

Assumption 3 (Measurable Phasing Variable): There exists a smooth and scalar global variable $\theta(x)$, referred to as the phasing variable, which satisfies the following conditions:

1) $\theta(x)$ is strictly monotonic along the periodic orbit $\mathcal{O}$.
2) The control input u does *not* explicitly appear in the equations of $\theta(x), \dot{\theta}(x), \cdots,$ and $\theta^{(r-1)}(x) := \frac{\mathrm{d}^{r-1}}{\mathrm{d}t^{r-1}}\theta(x)$.
3) The sequence of $\theta(x)$ and its time-derivatives up to the order $r - 1$, i.e.,

$$\Theta(x) := \left(\theta(x), \dot{\theta}(x), \cdots, \theta^{(r-1)}(x) \right)^{\top} \in \mathbb{R}^r \quad (8)$$

is measurable for *both* subsystems Σ_1 and Σ_2.

From item 1 of Assumption 3, the phasing variable can replace time which is a key to obtaining time-invariant decentralized feedback controllers. In particular, the phasing variable represents the progress of the system (i.e., robot) on the periodic orbit (i.e., walking gait). Reference [39] shows that the existence of a phasing variable follows directly from Assumption 1 on the periodic orbit. Item 2 states that the phasing variable $\theta(x)$ and the individual measurable global variables $\psi_i(x)$ for $i \in \{1, 2\}$ have the same relative degree r with respect to the control input u. The reason for this assumption will be clarified in Section II-F2. From item 3, $\Theta(x)$ forms a set of global variables measurable for both subsystems Σ_1 and Σ_2 to coordinate the local controllers. This item is not restrictive for models of bipedal walking. In particular, one can define a proper phasing variable based on the absolute stance hip angle in the sagittal plane. This angle θ and its first-order time-derivative $\dot{\theta}$ may be measured for the subsystem Σ_2 by the IMUs attached to the thigh links in Example 1. It is further reasonable to assume that this angle is available to the human (i.e., subsystem Σ_1) through proprioception.

Now we present the class of parameterized local controllers as follows:

$$u_i = \Gamma_i\left(x_i, \Theta(x), \Psi_i(x), \xi_i\right), \quad i \in \{1, 2\}, \quad (9)$$

in which $\Gamma_i : \mathcal{X}_i \times \mathbb{R}^r \times \mathbb{R}^{rv_i} \times \Xi_i \to \mathcal{U}_i$ is a smooth and nonlinear feedback law of local state variables x_i, the common measurable global variables $\Theta(x)$, the individual measurable global variables $\Psi_i(x)$ for the subsystem Σ_i, and *stabilizing local parameters* $\xi_i \in \Xi_i$. In our approach, ξ_i for $i \in \{1, 2\}$ are sets of adjustable parameters which will be tuned offline using the BMI optimization algorithms of

Sections IV and V for exponential and robust stabilization of the periodic orbit $\mathcal{O}$, respectively. In addition, $\Xi_i \subset \mathbb{R}^{p_i}$ denotes the *local parameter space*. We remark that the local controllers of (9) depend on *two* different sets of measurable global variables. The first set includes $\Theta(x)$ which is common to both subsystems and composed of the phasing variable $\theta(x)$ and its time-derivatives up to the order $r - 1$ to *coordinate* the local controllers on the periodic orbit. The second set includes the individual measurable global variables $\Psi_i(x)$ to *improve* the robust stability of the periodic orbit. For instance in Example 1, the prosthetic leg controller may improve the gait stability by having access to the Euler angles and their first-order time-derivatives provided by two IMUs attached to the thigh links.

Remark 3: For the case of Example 1, mathematical models for the local controller of the human part are not known. However, for the purpose of this paper, we assume that the local controller for the human part is a *phase-dependent* nonlinear controller in a similar manner to [30]. Furthermore, evidence suggests that the phase-dependent models can reasonably predict human joint behavior even across perturbations [49]. Consequently, it is better to show the local controllers of (9) in the following form:

$$u_1 = \Gamma_1\left(x_1, \Theta(x), \xi_1\right) \quad (10)$$
$$u_2 = \Gamma_2\left(x_2, \Theta(x), \Psi_2(x), \xi_2\right), \quad (11)$$

because the orientation is included in x_1 and the local controller for the human part does not have access to the data from the two IMUs, i.e., $\Psi_1(x) = \emptyset$. To have a unified notation, however, we make use of (9) for the remainder of this paper. We remark that the objective of this paper is to show that the local feedback control structure of (10) and (11) is capable of producing exponentially/robustly stable underactuated 3D bipedal walking gaits.

D. Closed-Loop Hybrid Model

By employing the parameterized and local nonlinear controllers of (9), the parameterized family of closed-loop hybrid models becomes (see Fig. 2)

$$\Sigma_{\xi}^{\mathrm{cl}} : \begin{cases} \dot{x} = f^{\mathrm{cl}}(x, \xi), & x^- \notin \mathcal{S} \\ x^+ = \Delta(x^-, \xi) + d, & x^- \in \mathcal{S}, \end{cases} \quad (12)$$

in which $\xi := (\xi_1^{\top}, \xi_2^{\top})^{\top} \in \Xi \subset \mathbb{R}^p$, $\Xi := \Xi_1 \times \Xi_2$, and $p := p_1 + p_2 = \dim(\xi)$. Furthermore, $f^{\mathrm{cl}}(x, \xi) := f(x) + g(x)\Gamma(x, \xi)$ represents the closed-loop vector field, where $\Gamma(x, \xi) := (\Gamma_1^{\top}, \Gamma_2^{\top})^{\top}$ is the global feedback control law.

Remark 4: In the closed-loop hybrid model of (12), the reset map Δ is also parameterized by the local controller parameters ξ. The reason for this parameterization is to extend the analysis to multi-phase hybrid systems in Section VII. In particular, these hybrid systems can be written in the form of (12), in which the reset map Δ is the composition of the flows for the remaining continuous- and discrete-time phases [50, Proposition 4]. Hence, Δ includes the controller parameters employed during the remaining continuous-time phases.
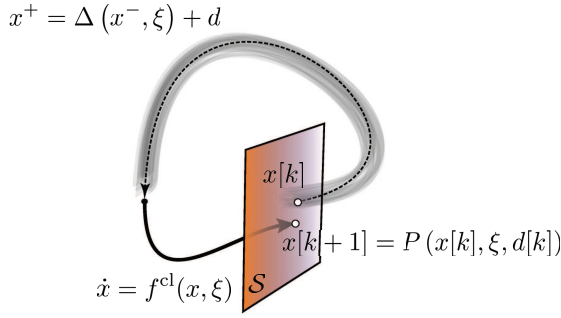
$$x^+ = \Delta\left(x^-, \xi\right) + d$$

Fig. 2: Illustration of the closed-loop hybrid model (12) and Poincaré return map [43]. The solid and dashed curves correspond to the flows of the continuous- and discrete-time dynamics $\dot{x} = f^{\mathrm{cl}}(x, \xi)$ and $x^+ = \Delta\left(x^-, \xi\right) + d$, respectively. The uncertainty in the discrete dynamics is shown by the cloud around the dashed curve.

For later purposes, the unique solution of the smooth and parameterized ODE $\dot{x} = f^{\mathrm{cl}}(x, \xi)$ with the initial condition $x(0) = x_0$ is given by $x(t) = \varphi(t, x_0, \xi)$ for all $t \geq 0$ in the maximal interval of existence. The *time-to-switching function* $T : \mathcal{X} \times \Xi \to \mathbb{R}_{>0}$ is also defined as the first time at which the flow $\varphi(t, x_0, \xi)$ intersects the switching manifold $\mathcal{S}$, i.e.,

$$T(x_0, \xi) := \inf\left\{t > 0 \,\middle|\, \varphi(t, x_0, \xi) \in \mathcal{S}\right\}. \tag{13}$$

E. Invariant Periodic Orbit

Throughout this paper, we shall assume that the parameterized family of local feedback laws in (9) preserves the periodic orbit in the sense that the orbit $\mathcal{O}$ is *invariant* under the choice of controller parameters ξ. This assumption becomes more clear as follows.

Assumption 4 (Invariant Periodic Orbit): It is assumed that $\mathcal{O}$ is an invariant periodic orbit for the closed-loop hybrid model (12) under the choice of controller parameters ξ. In particular, the following continuous- and discrete-time invariance properties are satisfied:

$$\frac{\partial f^{\mathrm{cl}}}{\partial \xi}(x, \xi) = 0, \quad \forall(x, \xi) \in \overline{\mathcal{O}} \times \Xi \tag{14}$$

$$\frac{\partial \Delta}{\partial \xi}(x^\star, \xi) = 0, \quad \forall \xi \in \Xi. \tag{15}$$

Assumption 4 allows us to employ the BMI optimization algorithms of Sections IV and V to search for stabilizing parameters ξ without changing the desired orbit $\mathcal{O}$.

F. Examples of Local Feedback Controllers

The objective of this section is to present two important families of local feedback controllers satisfying the invariance assumption.

1) Local LQR Controllers: The first family of feedback laws can be taken as local LQR controllers given by

$$\Gamma_i\left(x_i, \Theta(x), \Psi_i(x), \xi_i\right) =$$
$$u_i^\star(\theta) - \begin{bmatrix} K_{i1}(x_i, \xi_i) & K_{i2}(x_i, \xi_i) \end{bmatrix} \begin{bmatrix} x_i - x_{\mathrm{d},i}(\theta) \\ \Psi_i - \Psi_{\mathrm{d},i}(\theta) \end{bmatrix}, \tag{16}$$

in which

$$u_i^\star(\theta) = u_i^\star(t)\big|_{t = \boldsymbol{\theta}^{-1}(\theta)}$$

for $i \in \{1, 2\}$ represents the *local feedforward controller*, and $u_i^\star(t)$ is the nominal local control input for the subsystem Σ_i defined in Assumption 1. Furthermore, $\theta = \boldsymbol{\theta}(t)$ and $t = \boldsymbol{\theta}^{-1}(\theta)$ denote the time evolution of the phasing variable on the desired periodic orbit $\mathcal{O}$ and its inverse function, respectively. The desired evolutions of the local state variables x_i and individual measurable global variables Ψ_i on the orbit $\mathcal{O}$ versus the phasing variable θ are also represented by $x_{\mathrm{d},i}(\theta)$ and $\Psi_{\mathrm{d},i}(\theta)$. We note the local state-dependent gain matrices $K_{i1} \in \mathbb{R}^{m_i \times n_i}$ and $K_{i2} \in \mathbb{R}^{m_i \times rv_i}$ are parameterized by the local parameters ξ_i. It can easily be shown that the local controllers of (16) satisfy the continuous-time invariance condition in Assumption 4. We further remark that for the case of amputee locomotion, $\Psi_1(x) = \emptyset$, and hence, one needs to choose $K_{12}(x_1, \xi_1) \equiv 0$ to get the structure of the local controller given in (10).

2) Local Output Regulators: The second family of controllers includes local output regulators. In particular, for the subsystem Σ_i, one can define a *parameterized local output function* as follows:

$$y_i\left(x_i, \Theta(x), \Psi_i(x), \xi_i\right) = H_i(\xi_i)\left(x_i - x_{\mathrm{d},i}(\theta)\right) + \hat{H}_i(\xi_i)\left(\psi_i - \psi_{\mathrm{d},i}(\theta)\right), \tag{17}$$

in which $\dim(y_i) = \dim(u_i) = m_i$, and $H_i(\xi_i) \in \mathbb{R}^{m_i \times n_i}$ and $\hat{H}_i(\xi_i) \in \mathbb{R}^{m_i \times v_i}$ are *parameterized output matrices* to be determined. Here, $\psi_{\mathrm{d},i}(\theta)$ denotes the desired evolution of the individual global variable ψ_i on the periodic orbit $\mathcal{O}$ versus the phasing variable θ. We assume that these outputs have relative degree r with respect to the control input u on the periodic orbit $\mathcal{O}$ for all $\xi \in \Xi$. Then, the parameterized family of local output zeroing controllers can be chosen as[1]

$$\Gamma_i\left(x_i, \Theta(x), \Psi_i(x), \xi_i\right) = u_i^\star(\theta) - D_i^{-1}(x_i, \xi_i)\left(\sum_{j=0}^{r-1} k_j\, y_i^{(j)}\right), \tag{18}$$

where $D_i(x_i, \xi_i) \in \mathbb{R}^{m_i \times m_i}$ is a smooth and invertible local (lower-dimensional) decoupling matrix, and constants k_j for $j = 0, 1, \cdots, r-1$ are chosen such that the polynomial $\lambda^r + k_{r-1}\lambda^{r-1} + \cdots + k_1\lambda + k_0$ becomes Hurwitz. The family of local feedback laws in (18) represents an approximation for the centralized input-output (I-O) linearizing controllers of [51]. According to the construction procedure, the local output function y_i and its time-derivatives up to the order $r-1$ vanish on the desired periodic orbit $\mathcal{O}$, and hence, this family of controllers satisfies the invariance condition of Assumption 4. Finally, one can choose $\hat{H}_1 = 0$ to get the structure of the local controller given in (10).

---

[1]We remark that $y_i^{(j)} := \frac{\mathrm{d}^j y_i}{\mathrm{d}t^j}$ is a function of x_i, $(\theta, \dot{\theta}, \cdots, \theta^{(j)})$ and $(\psi_i, \dot{\psi}_i, \cdots, \psi_i^{(j)})$ for all $j = 0, 1, \cdots, r-1$. This underlines the importance of having $(\theta, \dot{\theta}, \cdots, \theta^{(r-1)})$ and $(\psi_i, \dot{\psi}_i, \cdots, \psi_i^{(r-1)})$ measurable for the subsystem Σ_i in Assumptions 2 and 3.

III. STABILIZATION PROBLEM

The objective of this section is to present the exponential and robust stabilization problems of the desired periodic orbit $\mathcal{O}$ for the closed-loop hybrid model (12). For this purpose, we make use of the method of Poincaré sections. By taking the Poincaré section as the switching manifold $\mathcal{S}$, the *parameterized Poincaré map* $P : \mathcal{X} \times \Xi \times \mathcal{D} \to \mathcal{X}$ is defined by

$$P(x, \xi, d) := \varphi\left(T\left(\Delta(x, \xi) + d, \xi\right), \Delta(x, \xi) + d, \xi\right), \quad (19)$$

which describes the evolution of the system on $\mathcal{S}$ according to the following discrete-time system (see Fig. 2):

$$\mathcal{P} : \begin{cases} x[k+1] = P(x[k], \xi, d[k]), & k = 0, 1, \cdots \\ c[k] = c(x[k]). \end{cases} \quad (20)$$

Here, $\{d[k]\}_{k=0}^{\infty}$ acts as a sequence of unknown disturbance inputs. Furthermore, $c[k]$ denotes a *set of smooth discrete-time controlled variables*. According to Assumption 4, $x^{\star}$ is an *invariant* fixed point for P in the absence of the disturbance input, i.e.,

$$P(x^{\star}, \xi, 0) = x^{\star}, \quad \forall \xi \in \Xi. \quad (21)$$

Linearization of the discrete-time system (20) around $(x^{\star}, d^{\star}) := (x^{\star}, 0)$ then yields

$$\partial\mathcal{P} : \begin{cases} \delta x[k+1] = \dfrac{\partial P}{\partial x}(x^{\star}, \xi, 0)\,\delta x[k] + \dfrac{\partial P}{\partial d}(x^{\star}, \xi, 0)\,d[k] \\ \qquad\qquad k = 0, 1, \cdots \\ \delta c[k] = C\,\delta x[k] \end{cases} \quad (22)$$

where $\delta x[k] := x[k] - x^{\star}$, $\delta c[k] := c[k] - c^{\star}$, $c^{\star} := c(x^{\star})$, and $C := \frac{\partial c}{\partial x}(x^{\star})$.

Problem 1 (Exponential Stability): The problem of exponential stabilization of the periodic orbit $\mathcal{O}$ consists of finding the controller parameters $\xi = (\xi_1^{\top}, \xi_2^{\top})^{\top}$ such that the Jacobian matrix $\frac{\partial P}{\partial x}(x^{\star}, \xi, 0)$ becomes Hurwitz.

Problem 2 (Robust Stability): The problem of robust stabilization of the periodic orbit $\mathcal{O}$ consists of finding the controller parameters ξ such that 1. the Jacobian matrix $\frac{\partial P}{\partial x}(x^{\star}, \xi, 0)$ becomes Hurwitz, and 2. the effect of the disturbance $d[k]$ on $\delta c[k]$ is attenuated.

Sections IV and V will solve the exponential and robust stabilization problems, respectively. For later purposes, we define the compact notations for the Jacobian matrices as $A(\xi) := \frac{\partial P}{\partial x}(x^{\star}, \xi, 0)$ and $B(\xi) := \frac{\partial P}{\partial d}(x^{\star}, \xi, 0)$ for which there are *not* in general closed-form expressions.

IV. ITERATIVE BMI ALGORITHM

This section creates a systematic numerical algorithm to overcome specific difficulties arising from the lack of a closed-form expression for the Poincaré map in tuning the decentralized feedback controllers of Section II-C. The algorithm is presented based on an iterative sequence of optimization problems to tune the parameters of the decentralized feedback control structure of (9), i.e., $\xi = (\xi_1^{\top}, \xi_2^{\top})^{\top}$, such that the desired orbit $\mathcal{O}$ becomes exponentially/robustly stable. Our iterative algorithm designs a sequence of controller parameters $\{\xi^{\ell}\}$, where the superscript $\ell \in \{0, 1, \cdots\}$ represents the

iteration number. The objective is then to converge to a set of parameters ξ^{ℓ} that solves Problems 1 and 2. This section deals with the exponential stabilization problem. Section V will extend the algorithm for robust stabilization. In what follows, we present the steps of the algorithm.

A. Step 1: Sensitivity Analysis

During the iteration number $\ell \in \{0, 1, \cdots\}$, the sensitivity analysis replaces the Jacobian matrices $A(\xi^{\ell} + \Delta\xi)$ and $B(\xi^{\ell} + \Delta\xi)$ with their first-order approximations based on the Taylor series expansion, that is,

$$\begin{aligned} A\left(\xi^{\ell} + \Delta\xi\right) &\approx A\left(\xi^{\ell}\right) + \bar{A}\left(\xi^{\ell}\right)\left(I_n \otimes \Delta\xi\right) \\ &=: \hat{A}\left(\xi^{\ell}, \Delta\xi\right) \end{aligned} \quad (23)$$

$$\begin{aligned} B\left(\xi^{\ell} + \Delta\xi\right) &\approx B\left(\xi^{\ell}\right) + \bar{B}\left(\xi^{\ell}\right)\left(I_n \otimes \Delta\xi\right) \\ &=: \hat{B}\left(\xi^{\ell}, \Delta\xi\right). \end{aligned} \quad (24)$$

Here, $\Delta\xi \in \mathbb{R}^p$ is a sufficiently small increment in controller parameters, I_n is the identity matrix of the order[2] n, "$\otimes$" represents the Kronecker product, and $\bar{A}(\xi^{\ell})$ and $\bar{B}(\xi^{\ell})$ denote the *sensitivity matrices with respect to* ξ, evaluated at $\xi = \xi^{\ell}$. Systematic numerical approaches to calculate the sensitivity matrices based on the continuous-time ODE and reset map have been presented in [41, Theorems 1 and 2].

The sensitivity analysis returns approximate Jacobian matrices with closed-form expressions, which are affine in $\Delta\xi$, and then translates the stabilization problem into an approximate one that is easier to solve through a set of LMIs and BMIs.

Problem 3 (Approximate Exponential Stability): The problem of approximate exponential stabilization during the iteration number ℓ consists of finding the increment in controller parameters $\Delta\xi^{\ell}$ such that the approximate Jacobian matrix $\hat{A}(\xi^{\ell}, \Delta\xi^{\ell})$ becomes Hurwitz.

B. Step 2: BMI Optimization Problem

The objective of the BMI optimization problem during the iteration $\ell \in \{0, 1, \cdots\}$ is to search for the increment in controller parameters $\Delta\xi^{\ell}$ such that the requirements of Problem 3 are satisfied. We make use of the BMI optimization framework of [41, Theorem 1] to make the approximate Jacobian matrix $\hat{A}(\xi^{\ell}, \Delta\xi^{\ell})$ Hurwitz. However, unlike [41], we apply the BMI optimization in an iterative manner[3]. In particular, we set up the following optimization problem during the iteration

---

[2]For the closed-loop hybrid model (12), the Poincaré map is in fact an $n - 1$ dimensional return map which maps the system's state from the $n - 1$ dimensional switching manifold $\mathcal{S}$ back to $\mathcal{S}$. Hence, $A(\xi)$ is an $(n - 1) \times (n - 1)$ matrix. However to simplify the notation for the remaining of the paper, we assume that $A(\xi)$ is $n \times n$.

[3]We have observed that for decentralized control problems the BMI optimization algorithm must be applied iteratively to converge to a stabilizing solution.

number ℓ:

$$\min_{W, \Delta\xi, \mu, \eta} - w\,\mu + \eta \tag{25}$$

$$\text{s.t.} \quad \begin{bmatrix} W & \hat{A}\left(\xi^\ell, \Delta\xi\right) W \\ \star & (1-\mu)\,W \end{bmatrix} > 0 \tag{26}$$

$$\begin{bmatrix} I_p & \Delta\xi \\ \star & \eta \end{bmatrix} > 0 \tag{27}$$

$$\mu > 0, \tag{28}$$

in which $W = W^\top \in \mathbb{R}^{n \times n}$ is a positive definite matrix, and $\mu > 0$ is scalar to tune the spectral radius of $\hat{A}(\xi^\ell, \Delta\xi)$. The matrix inequality (26) represents a BMI condition because of the product of $\hat{A}(\xi^\ell, \Delta\xi)$ and W. Using Schur's complement lemma, it can be shown that $V(\delta x[k]) := \delta x[k]^\top W^{-1} \delta x[k]$ is a Lyapunov function for the approximate model $\delta x[k+1] = \hat{A}(\xi^\ell, \Delta\xi)\delta x[k]$ which satisfies $V[k+1] - V[k] < -\mu V[k]$. It can also be shown that $\sqrt{1-\mu}$ is an upper bound for the spectral radius of $\hat{A}(\xi^\ell, \Delta\xi)$. Finally, (27) is an LMI condition in which using Schur's complement lemma, one can consider η as a dynamic upper bound for $\|\Delta\xi\|_2^2$, that is, $\eta > \|\Delta\xi\|_2^2$. The cost function then tries to minimize a linear combination of $-\mu$ and η with the positive weighting factor w to improve the spectral radius and to have a good approximation based on the truncated Taylor series expansion in (23).

C. Step 3: Iteration

Let $(W^\star, \Delta\xi^\star, \mu^\star, \eta^\star)$ represent a *local*[4] minimum for the BMI optimization problem (25)-(28). Next, define $\Delta\xi^\ell := \Delta\xi^\star$ and update the controller parameters as follows

$$\xi^{\ell+1} = \xi^\ell + \Delta\xi^\ell. \tag{29}$$

If the requirement of the real exponential stabilization problem (i.e., Problem 1) is satisfied at $\xi = \xi^{\ell+1}$, the algorithm is successful and stops. Otherwise, it continues by coming back to Step 1 (Sensitivity Analysis) around the updated parameters $\xi^{\ell+1}$ and going through the next steps. In case the BMI optimization problem of Step 2 is not feasible, the algorithm is not successful and stops. Section VI will present sufficient conditions for the convergence of the algorithm to a stabilizing solution.

V. ROBUST STABILIZATION

The objective of this section is to extend the iterative BMI algorithm of Section IV to address the robust stabilization problem of the periodic orbit $\mathcal{O}$. In particular, after finding an exponentially stabilizing decentralized feedback control solution, one can apply the extended algorithm to improve the robust stability behavior. For this purpose, we first define an approximate robust stabilization problem during the iteration $\ell \in \{0, 1, \cdots\}$ as follows.

Problem 4 (Approximate Robust Stability): The problem of approximate robust stabilization consists of finding the increment in controller parameters $\Delta\xi^\ell$ such that 1. the approximate

---

[4]More details about local solutions of the BMI optimization problem (25)-(28) will be presented in Section VII-B.

Jacobian matrix $\hat{A}(\xi^\ell, \Delta\xi^\ell)$ becomes Hurwitz, and 2. the $\mathcal{H}_2$-norm of the transfer function $T_{dc}(z)$, relating the disturbance input $d[k]$ to the controlled outputs $\delta c[k]$ in the approximate linearized model

$$\partial\hat{\mathcal{P}} : \begin{cases} \delta x[k+1] = \hat{A}\left(\xi^\ell, \Delta\xi^\ell\right)\,\delta x[k] + \hat{B}\left(\xi^\ell, \Delta\xi^\ell\right)\,d[k] \\ \qquad k = 0, 1, \cdots \\ \qquad \delta c[k] = C\,\delta x[k], \end{cases} \tag{30}$$

becomes less that $\sqrt{\mu}$. That is,

$$\|T_{dc}\|_{\mathcal{H}_2}^2 := \frac{1}{2\pi}\int_{-\pi}^{\pi} \text{trace}\left(T_{dc}^{\mathsf{H}}\left(e^{j\omega}\right) T_{dc}\left(e^{j\omega}\right)\right) \mathrm{d}\omega < \mu, \tag{31}$$

where "trace" and the superscript "H" denote the trace and conjugate transpose of a matrix, respectively.

To solve Problem 4, we then replace the BMI optimization problem in Step 2 of the iterative algorithm with the extended one as follows:

$$\min_{W, Z, \Delta\xi, \mu, \eta} w\,\mu + \eta \tag{32}$$

$$\text{s.t.} \quad \begin{bmatrix} W & \hat{A}\left(\xi^\ell, \Delta\xi\right) W & \hat{B}\left(\xi^\ell, \Delta\xi\right) \\ \star & W & 0 \\ \star & \star & I \end{bmatrix} > 0 \tag{33}$$

$$\begin{bmatrix} W & C\,Z \\ \star & Z \end{bmatrix} > 0 \tag{34}$$

$$\begin{bmatrix} I & \Delta\xi \\ \star & \eta \end{bmatrix} > 0 \tag{35}$$

$$\text{trace}\,(W) < \mu, \tag{36}$$

in which $W = W^\top$, $Z = Z^\top$, $\Delta\xi$, μ, and η are new decision variables. In addition, $\Delta\xi^\ell$ in Step 3 of the algorithm is set to $\Delta\xi^\star$, where $\Delta\xi^\star$ denotes the local optimal solution of the problem (32)-(36). From [52, Lemma 1], the BMI condition (33) in combination with the LMIs (34) and (36) are equivalent to the matrix $\hat{A}(\xi^\ell, \Delta\xi)$ being Hurwitz and $\|T_{dc}\|_{\mathcal{H}_2}^2 < \mu$. In addition, similar to the BMI optimization problem (25)-(28), the LMI condition (35) presents the dynamic upper bound η on $\|\Delta\xi\|_2^2$ to have a good approximation based on the truncated Taylor series expansion in (23) and (24). Finally, the cost function minimizes a linear combination of the $\mathcal{H}_2$ control parameter μ and the dynamic upper bound η with the positive weighting factor w. One can stop the extended iterative algorithm when 1. the real Jacobian matrix $A(\xi^{\ell+1})$ becomes Hurwitz, and 2. the $\mathcal{H}_2$-norm of the transfer function relating $d[k]$ to $\delta c[k]$ in the real linearized model (22) is less than a desired value.

VI. SUFFICIENT CONDITIONS FOR THE CONVERGENCE OF THE BMI ALGORITHMS

The objective of this section is to present sufficient conditions under which the iterative BMI algorithms stabilize the periodic orbit $\mathcal{O}$ for the closed-loop hybrid model (12) at a finite number of iterations. These conditions are expressed in terms of the first-, second-, or third-order derivatives of the Poincaré map. The exponential stabilization problem is

first investigated in Theorems 1 and 2. Then, the results are extended to the $\mathcal{H}_2$ control problem in Theorem 3. For this purpose, we present a *non-smooth* optimization problem which is equivalent to the BMI optimization problem (25)-(28). We remark that we do *not* numerically solve this non-smooth optimization problem during the iterative algorithm. However, we make use of it for the proof of convergence.

Lemma 1 (Equivalent Non-smooth Problem): The BMI optimization problem (25)-(28) is equivalent to the following non-smooth problem

$$\min_{\Delta\xi,\gamma} \frac{1}{2} w\,\gamma^2 + \frac{1}{2}\,\|\Delta\xi\|_2^2 \tag{37}$$

$$\text{s.t.} \quad \rho\left(\hat{A}\left(\xi^\ell, \Delta\xi\right)\right) < \gamma \tag{38}$$

$$\gamma < 1, \tag{39}$$

in which $\rho(.)$ denotes the spectral radius of a matrix.

Proof: See Appendix A. ∎

For later purposes, let us define $a(\xi) := \text{vec}(A(\xi)) \in \mathbb{R}^{n^2}$, in which "vec" denotes the vectorization operator. In a similar manner, one can define $\hat{a}(\xi^\ell, \Delta\xi) := \text{vec}(\hat{A}(\xi^\ell, \Delta\xi)) \in \mathbb{R}^{n^2}$ as the first-order approximation of $a(\xi^\ell + \Delta\xi)$.

A. Scalar Case

For the scalar case (i.e., $n = 1$), we can present a closed-form expression for the global optimal solution of the equivalent problem (37)-(39). This helps us to investigate the sufficient conditions for the convergence of the iterative algorithm. In particular, we present the following result.

Theorem 1 (Convergence of the Algorithm for $n=1$): Consider the smooth function $a : \mathbb{R} \to \mathbb{R}$ by $a(\xi)$. Suppose further that there exists $\bar{\xi} \in \mathbb{R}$ such that $a(\bar{\xi}) = 0$. Let $\mathcal{B}$ denote a compact (i.e., closed and bounded) ball around $\bar{\xi}$ such that (1) $a'(\xi) := \frac{da}{d\xi}(\xi) \neq 0$ for all $\xi \in \mathcal{B}$, and (2)

$$\max_{\xi \in \mathcal{B}} \frac{|a(\xi)|}{w\,(a'(\xi))^2 + 1} < 1. \tag{40}$$

Then, there exist $\delta > 0$ and $0 < N < \infty$ such that for all initial guesses of the BMI algorithm $\xi^0 \in \mathcal{B}$ with the property $|\xi^0 - \bar{\xi}| < \delta$, the global solution of the BMI optimization problem (25)-(28) results in the following parameter update law

$$\xi^{\ell+1} = \xi^\ell - \frac{w\,a\left(\xi^\ell\right) a'\left(\xi^\ell\right)}{w\,(a'\left(\xi^\ell\right))^2 + 1} =: Q\left(\xi^\ell\right). \tag{41}$$

Furthermore, the update law (41) stabilizes the origin for the discrete-time system $\delta x[k+1] = a(\xi)\,\delta x[k]$ at a finite number of iterations, that is, $|a(\xi^\ell)| < 1$ for all $\ell > N$.

Proof: See Appendix B. ∎

Remark 5: Theorem 1 presents a set of sufficient conditions under which one can find the global optimal solution for the BMI optimization problem (25)-(28). Moreover, it investigates the convergence of the algorithm to a stabilizing solution. The conditions of this theorem are not restrictive. In particular, the condition $a'(\xi) \neq 0$ for all $\xi \in \mathcal{B}$ guarantees the feasibility of the BMI condition in (26) for the scalar case and looks like a similar condition for Newton's method. The second condition, in (40), can easily be achieved by choosing a large

weighting factor $w > 0$. Furthermore for sufficiently large w, one can show that the recursive law (41) reduces to the Newton's method, i.e., $\xi^{\ell+1} = \xi^\ell - \frac{a(\xi^\ell)}{a'(\xi^\ell)}$.

B. Multi-Dimensional Case

For the multi-dimensional case (i.e., $n > 1$), there is *not* a closed-form expression for the global/local optimal solution of the BMI optimization problem (25)-(28) or the equivalent problem (37)-(39) to investigate the sufficient conditions for the convergence of the algorithm similar to those presented in Theorem 1. However, from Lemma 1 we can still present an alternative set of sufficient conditions based on the concept of *convexity* to guarantee the convergence of the algorithm at a finite number of iterations. In particular, we guarantee the stability of the real Jacobian matrix during the iteration $\ell + 1$ based on some mild conditions on the *local* optimal solution of the BMI optimization problem during the iteration ℓ. To make this notion more precise, let $\chi(z) := \det(zI - A)$ denote the characteristic equation of a given $n \times n$ matrix A. Next, $\rho(A) < \gamma$ for some $\gamma > 0$ is equivalent to the matrix $\frac{1}{\gamma}A$ being Hurwitz which is also equivalent to the monic polynomial $\frac{1}{\gamma^n}\chi(\gamma z) = \det(zI - \frac{1}{\gamma}A)$ being Hurwitz. From the Jury stability criterion, this is equivalent to the existence of a smooth function $F : \mathbb{R}^{n^2} \times \mathbb{R}_{>0} \to \mathbb{R}^{n+1}$ such that

$$F_\alpha(a, \gamma) < 0, \quad \alpha = 1, 2, \cdots, n+1,$$

where $a = \text{vec}(A) \in \mathbb{R}^{n^2}$. Appendix C presents a systematic approach to construct the function $F(a, \gamma)$ based on the Jury array. Now we are in a position to present the following result.

Theorem 2 (Convergence of the Algorithm for $n > 1$): Consider the smooth matrix $A(\xi) \in \mathbb{R}^{n \times n}$ and assume that the BMI optimization problem (25)-(28) is feasible during the iteration ℓ. Suppose further that $(\Delta\xi^\star, \mu^\star)$ denotes a *local* optimal solution (*not* necessarily the global solution). Then there is $\epsilon > 0$ such that if (1) $\|\Delta\xi^\star\| < \epsilon$, and (2) the condition

$$\sum_{\beta=1}^{n^2} \frac{\partial F_\alpha}{\partial a_\beta}\left(a\left(\xi^\ell\right), \sqrt{1-\mu^\star}\right) \frac{\partial^2 a_\beta}{\partial\xi^2}\left(\xi^\ell\right) \leq 0 \tag{42}$$

for $\alpha = 1, \cdots, n+1$ is satisfied, then the algorithm terminates at the iteration $\ell + 1$ in the sense that $A(\xi^\ell + \Delta\xi^\star)$ becomes Hurwitz. Here, $a_\beta(\xi)$ represents the β-th component of $a(\xi)$ and $\frac{\partial^2 a_\beta}{\partial\xi^2}(\xi)$ is the corresponding Hessian matrix for $\beta = 1, \cdots, n^2$.

Proof: See Appendix D. ∎

Remark 6: By defining the scalar coefficients $\nu_{\alpha\beta} := \frac{\partial F_\alpha}{\partial a_\beta}\left(a\left(\xi^\ell\right), \sqrt{1-\mu^\star}\right)$ for $\alpha = 1, \cdots, n+1$ and $\beta = 1, \cdots, n^2$, the condition (42) can be expressed as

$$\sum_{\beta=1}^{n^2} \nu_{\alpha\beta} \frac{\partial^2 a_\beta}{\partial\xi^2}\left(\xi^\ell\right) \leq 0, \quad \alpha = 1, \cdots, n+1, \tag{43}$$

which is a set of $n+1$ LMIs in terms of n^2 Hessian matrices $\frac{\partial^2 a_\beta}{\partial\xi^2}\left(\xi^\ell\right)$, $\beta = 1, \cdots, n^2$. We remark that one can interpret the inequality (43) as a set of convexity conditions on the elements of the Jacobian matrix $A(\xi)$ at $\xi = \xi^\ell$.

C. Extension to the $\mathcal{H}_2$ Problem

This section extends the sufficient conditions of Theorem 2 to the convergence of the extended BMI algorithm at a finite number of iterations. In particular, we express a set of $n+2$ convexity conditions in terms of the elements of the Jacobian matrices $A(\xi)$ and $B(\xi)$ at $\xi = \xi^\ell$.

Theorem 3 (Convergence of the Extended Algorithm): Consider the smooth matrices $A(\xi) \in \mathbb{R}^{n \times n}$ and $B(\xi) \in \mathbb{R}^{n \times n}$ and define $a(\xi) = \text{vec}(A(\xi))$ and $b(\xi) = \text{vec}(B(\xi))$. Assume that the BMI optimization problem (32)-(36) is feasible during the iteration number ℓ and let $(\Delta \xi^\star, \mu^\star)$ denote a *local* optimal solution. Then there is $\epsilon > 0$ and coefficients $\overline{v}_{\alpha\beta}$ and $\underline{v}_{\alpha\beta}$ for $\alpha = 1, \cdots, n+2$ and $\beta = 1, \cdots, n^2$ such that if (1) $\|\Delta\xi^\star\| < \epsilon$ and (2) the following convexity requirements on the Hessian matrices $\frac{\partial^2 a_\beta}{\partial \xi^2}(\xi)$ and $\frac{\partial^2 b_\beta}{\partial \xi^2}(\xi)$ are satisfied

$$\sum_{\beta=1}^{n^2} \left\{ \overline{v}_{\alpha\beta} \frac{\partial^2 a_\beta}{\partial \xi^2} \left(\xi^\ell \right) + \underline{v}_{\alpha\beta} \frac{\partial^2 b_\beta}{\partial \xi^2} \left(\xi^\ell \right) \right\} \le 0, \tag{44}$$

$$\alpha = 1, \cdots, n+2,$$

then 1. the real Jacobian matrix $A(\xi^\ell + \Delta\xi^\star)$ becomes Hurwitz and 2. the $\mathcal{H}_2$-norm of the transfer function for the quadruple $(A(\xi^\ell + \Delta\xi^\star), B(\xi^\ell + \Delta\xi^\star), C, 0)$ in the real model (22) is less than $\sqrt{\mu^\star}$.

Proof: See Appendix E. ∎

Remark 7: Under Assumptions 1-4, if the conditions of Theorems 2 and 3 are satisfied for any decentralized feedback law as given in (9), then the algorithm can exponentially/robustly stabilize the periodic orbit $\mathcal{O}$ for the closed-loop hybrid model.

VII. APPLICATION TO ROBOTIC WALKING

Virtual constraints are kinematic relations among the generalized coordinates of mechanical systems that are enforced asymptotically by continuous-time controllers [2], [3], [11], [28], [29], [41], [42], [53]–[57]. They are defined to coordinate the links of bipedal robots within a stride. In particular, virtual constraints are defined as holonomic output functions $y(x)$ for continuous-time portions of hybrid models of walking and they are typically enforced (i.e., $y \equiv 0$) by *centralized* I-O linearizing feedback laws [51]. Virtual constraint controllers have been numerically and experimentally validated for stable 2D and 3D underactuated bipedal robots [14], [53]–[55], [58] as well as 2D powered prosthetic legs [28]–[30], [47]. For mechanical systems with more than one degree of underactuation, the stability of the periodic gait depends on the choice of the virtual constraints [13], [41].

The application of virtual constraints to amputee locomotion presents some challenges not previously encountered in autonomous bipedal robots. In particular, centralized virtual constraint controllers would require state feedback from the human body. To overcome interacting forces between two subsystems, [28] has implemented virtual constraint controllers using local *high-gain controllers* in simulations of a 2D powered prosthetic leg, but safety concerns limited the experimental implementation to inaccurate low-gain controllers.
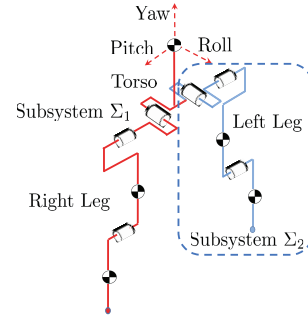

Fig. 3: The structure of the 9 DOFs autonomous bipedal robot. The model consists of a tree structure with a torso and two identical legs with three unactuated Euler angles and 6 actuated revolute joints. Subsystems Σ_1 (human part) and Σ_2 (prosthetic part) with the corresponding DOFs have been shown in the figure.

The local output functions for the prosthetic subsystem were also defined based on a *physical intuition*. A recent approach measures the human interaction forces for exact local virtual constraint control [30]. In particular, the feedback from force sensors is used to cancel the nonlinear interaction terms between the human and prosthetic subsystems in the feedback linearization approach. However, multi-axis force sensors that are light enough for prosthetic limbs are extremely expensive.

There is currently no systematic algorithm to design decentralized virtual constraints to induce stable and underactuated 3D walking gaits in bipedal robots and powered prosthetic legs. The objective of this section is to employ the iterative BMI algorithm of Sections IV and V to search for robust stabilizing local virtual constraints. We remark that the BMI algorithm takes into account the interactions between the two subsystems in the full model while searching for the optimized local virtual constraints, preventing the need to employ impractical high-gain controllers, expensive force sensors, or asymptotic observers to deal with interactions.

A. Underactuated 3D Bipedal Model

We consider an underactuated 3D bipedal robot and employ the iterative BMI algorithm to tune the decentralized virtual constraints to induce an exponentially stable walking gait. The model of the robot forms a tree structure consisting of a torso link and two identical legs terminating at point feet (see Fig. 3). Each leg of the robot includes 3 actuated DOFs: a 2 DOF hip (ball) joint with roll and pitch angles plus a 1 DOF knee joint. During the single support phase, the robot has 9 DOFs including 6 actuated DOFs of two legs and 3 unactuated DOFs corresponding to the absolute orientation of the torso with respect to the world frame. To describe this orientation, we attach a frame to the torso with the y-axis being in the direction of walking and the z-axis being upward. Then, the orientation of the torso frame can be described by three Euler angles, referred to as the *yaw*, *roll*, and *pitch* angles. The kinematic and dynamic parameter values for the links are taken according to those reported in [59] for a 3D human model.

The state vector for the mechanical system can be chosen as $x := (q^\top, \dot{q}^\top)^\top \in \mathcal{X} \subset \mathbb{R}^{18}$, in which q and $\dot{q}$ denote the generalized coordinates and velocity vectors, respectively. The control inputs are also shown by $u \in \mathcal{U} \subset \mathbb{R}^6$ to represent the motor torques applied at the actuated joints. The hybrid model of walking includes two continuous-time phases to represent the right and left stance phases and two discrete-time phases to represent the right-to-left and left-to-right impact models. In particular, we study the following two-phase hybrid model

$$\begin{aligned} \Sigma_\text{R} : & \begin{cases} \dot{x} = f_\text{R}(x) + g_\text{R}(x)\, u, & x^- \notin \mathcal{S}_{\text{R}\to\text{L}} \\ x^+ = \Delta_{\text{R}\to\text{L}}(x^-), & x^- \in \mathcal{S}_{\text{R}\to\text{L}} \end{cases} \\ \Sigma_\text{L} : & \begin{cases} \dot{x} = f_\text{L}(x) + g_\text{L}(x)\, u, & x^- \notin \mathcal{S}_{\text{L}\to\text{R}} \\ x^+ = \Delta_{\text{L}\to\text{R}}(x^-), & x^- \in \mathcal{S}_{\text{L}\to\text{R}}, \end{cases} \end{aligned} \quad (45)$$

in which the subscripts "R", "L", "R $\to$ L", "L $\to$ R" denote the right stance phase, left stance phase, right-to-left impact, and left-to-right impact, respectively. The continuous-time phases $\dot{x} = f_\text{R}(x) + g_\text{R}(x)\, u$ and $\dot{x} = f_\text{L}(x) + g_\text{L}(x)\, u$ are constructed based on the Lagrangian dynamics, whereas the discrete-time transitions $x^+ = \Delta_{\text{R}\to\text{L}}(x^-)$ and $x^+ = \Delta_{\text{L}\to\text{R}}(x^-)$ assume rigid and instantaneous contact models [60]. Using [50, Proposition 4], one can obtain an equivalent single-phase hybrid system, as given in (1), for the two-phase model (45). For this purpose, without loss of generality, the continuous-time portion $\dot{x} = f(x) + g(x)\, u$ can be constructed based on the right stance phase dynamics. In addition, the discrete-time portion $x^+ = \Delta(x^-)$ is taken as the composition of the right-to-left impact, left stance phase, and left-to-right impact models. In this model, the uncertainty $d[k]$ in (1) can arise from uncertainties in the impact maps and the flow of the left stance phase. A desired periodic gait $\mathcal{O}$ is then designed using the motion planning algorithm of [14] for walking at 0.6 (m/s) with the cost of mechanical transport CMT = 0.07.

Motivated by a transpelvic amputee (the "human" part) walking with a prosthetic left leg, we consider a two-part decentralization scheme as shown in Fig 3. The prosthetic subsystem Σ_2 includes the 3 DOFs of the left leg with the corresponding 3 actuators, and hence, $\dim(x_2) = 6$ and $\dim(u_2) = 3$. In particular, $x_2 = (q_2^\top, \dot{q}_2^\top)^\top$, in which q_2 and $\dot{q}_2$ denote the generalized position and velocity vectors for the left leg, respectively. The human subsystem Σ_1 then consists of the rest of the model, including the torso and right leg, with $\dim(x_1) = 12$ and $\dim(u_1) = 3$. In addition, $x_1 = (q_1^\top, \dot{q}_1^\top)^\top$, where q_1 and $\dot{q}_1$ represent the generalized position and velocity vectors for Σ_1. Since the local state variables x_1 already include the orientation variables, i.e., torso Euler angles and their first-order time-derivatives, the set of measurable global variables for Σ_1 is chosen as empty, i.e., $\Psi_1(x) = \emptyset$. However, the set of measurable global variables $\Psi_2(x) = (\psi_2^\top(x), \dot{\psi}_2^\top(x))^\top$ for the subsystem Σ_2 includes two roll and two yaw angles as well as their velocities provided by the IMUs attached to both thighs (i.e., $\dim(\psi_2) = 4$ and $\dim(\Psi_2) = 8$).

For the purpose of this paper, the decentralized virtual constraints are defined as (17). We only remark that they need to be holonomic quantities and consequently, one would need to replace x_i and $x_{\text{d},i}(\theta)$ in (17) with the local configuration

variables q_i and the corresponding desired evolution $q_{\text{d},i}(\theta)$, respectively for $i \in \{1, 2\}$. Next the local output matrices to be determined include $H_1(\xi_1) \in \mathbb{R}^{3\times 6}$, $H_2(\xi_2) \in \mathbb{R}^{3\times 3}$, and $\hat{H}_2(\xi_2) \in \mathbb{R}^{3\times 4}$, or equivalently 39 parameters (we note that $\hat{H}_1 = 0$ to get the structure of (10)). Moreover, since the typical walking period includes two steps, we need to determine these matrices for the right and left stance phases and therefore, the total number of parameters is $39 \times 2 = 78$, i.e., $\xi \in \mathbb{R}^{78}$. The lower-dimensional decoupling matrices in (18) are also taken as constant matrices. This reduces the local controllers of (18) into a set of *PD controllers* ($r = 2$) for which the choice of local output functions guarantees the robust stability of the orbit. The outputs are then systematically chosen according to the iterative BMI algorithms.

Remark 8: Although legged robots are becoming more nonlinear with higher DOFs, the centralized nonlinear control methods required to achieve stable locomotion *cannot scale* with the dimensionality of these robots. Most centralized nonlinear control methods, e.g., feedback linearization, require the inversion of a state-dependent "decoupling" matrix in real time [2], [4], [13], [41], but the computational complexity of this operation scales quadratically with matrix dimension [61], corresponding to the number of DOFs in the robot. Moreover, inverting the full decoupling matrix distributes (and amplifies) local modeling errors across all DOFs in the closed-loop dynamics. This curse of dimensionality presents a key roadblock to the application of traditional centralized nonlinear controllers to increasingly sophisticated legged robots. We remark that the proposed approach reduces the local controllers of (18) into a set of PD controllers for which the choice of the output functions plays an important role in the gait stabilization process.

B. PENBMI Solver and Numerical Results

Unlike LMIs, BMIs are non-convex and NP-hard problems [62]. However, PENBMI is a general-purpose solver for BMIs which guarantees the convergence to a local optimal point satisfying the Karush Kuhn Tucker optimality conditions [63]. To solve the BMI optimization problems at each iteration of the algorithms presented in Sections IV and V, we make use of the PENBMI solver from TOMLAB [64] integrated with the MATLAB environment through YALMIP [65].

1) Exponential Stabilization Problem: An initial set of controller parameters $\xi^0 \in \mathbb{R}^{78}$ is assumed based on a physical intuition for the local output functions (17). For this set of parameters, the dominant eigenvalues and spectral radius of the 17×17 Jacobian matrix of the Poincaré map become $\{0.12029 \pm 1.7223i, -0.4863, -0.4178\}$ and 1.7253, respectively, and therefore the periodic gait $\mathcal{O}$ is not stable. To exponentially stabilize the gait, we make use of the iterative BMI algorithm developed in Section IV with the weighting factor $w = 0.1$. The algorithm successfully converges to a set of stabilizing parameters after 3 iterations, where the BMI optimization problem of each iteration takes approximately 15 minutes on a dual 2.3 GHz Intel Xeon E5-2670 v3 processor. For the BMI optimized solution, the dominant eigenvalues and spectral radius of the Jacobian of the Poincaré map become

$\{-0.4747\pm0.4445i, 0.5028, 0.3628\}$ and 0.6503 (i.e., 62.31% improvement in the spectral radius), respectively. Starting from the same initial guess with the different weighting factors $w = 0.5$ ad $w = 0.05$, the algorithm converges to alternative stabilizing solutions with the spectral radii 0.7215 and 0.6135 after 2 and 3 iterations, respectively.

2) Robust Stabilization Problem: To robustly stabilize the periodic orbit $\mathcal{O}$ against the discrete-time uncertainties in the impact model, we define a set of discrete-time outputs $c[k] = c(x[k])$ on the Poincaré section (i.e., the right-to-left switching manifold) as the robot's COM velocity along the x-, y-, and z-axes of the world frame. The $\mathcal{H}_2$-norm of the transfer function relating $d[k]$ to $\delta c[k]$ in the linearized model (22) for the previous BMI optimized solution (with $w = 0.1$) is 29.7234. Starting with this exponentially stable solution, we employ the extended BMI algorithm of Section V to reduce the $\mathcal{H}_2$-norm. By choosing $w = 0.1$, the extended algorithm converges to a robust stabilizing solution after 3 iterations for which the $\mathcal{H}_2$-norm becomes 12.8860 (56.65% improvement in the $\mathcal{H}_2$-norm). Figure 4 depicts the phase portraits for the torso Euler angles and frontal prosthetic hip angle during 100 consecutive walking steps with the robust stabilizing solution. The orbit $\mathcal{O}$ has been designed to walk along the y-axis of the world frame which corresponds to the yaw angle being zero. Here, the simulation starts off of the orbit at the beginning of the right stance phase. Convergence to the periodic orbit, even in the yaw position, can be seen from the phase portraits. The animation of this simulation can be found at [66].

C. Robustness Against Impact Model Uncertainties

The objective of this section is to compare the performances of the two BMI-optimized solutions of Sections VII-B1 and VII-B2 against the impact model uncertainty $d[k]$. For this purpose, a randomly generated discrete-time disturbance input $d[k]$ is assumed in the velocity components of the impact models. Fig. 5 illustrates the corresponding x, y and z components of the deviation in the robot's COM velocity (i.e., $\delta c[k]$) for the stability-optimized and robustness-optimized local controllers. It is clear that the BMI-optimized solution for the $\mathcal{H}_2$-norm has better performance compared to the one optimized only for the stability.

D. Robustness Against Nonparametric Uncertainties and Contact Models

The objective of this section is to show that the robust decentralized control strategy will result in stable walking motions even if the assumptions made in modeling of the hybrid system are not met exactly. In particular, we consider nonparametric uncertainties in the model of the robot. In (45), the evolution of the robot is described by a *rigid* two-phase hybrid model consisting of the right and left stance phases as well as the right-to-left and left-to-right impact models (i.e., instantaneous double support phases). This section presets a *continuous* and *compliant model* to describe the evolution of the walking motion during the single and non-instantaneous double support phases [67]. Here, we make use of the LuGre model [68] to represent forces between the contacting surfaces.
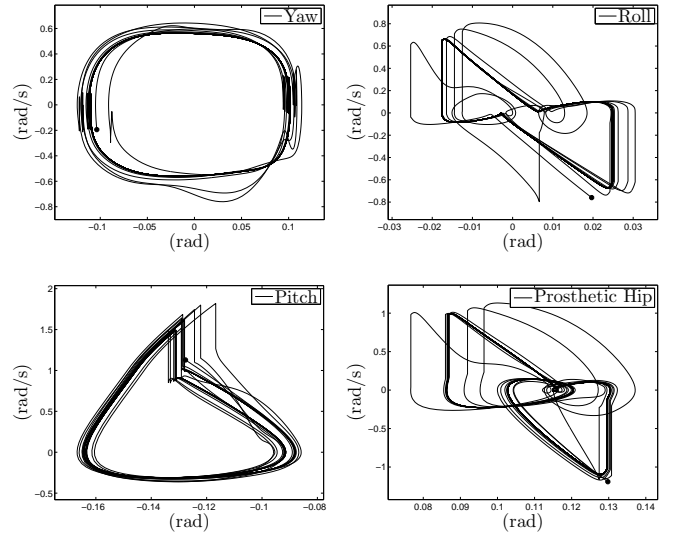

Fig. 4: Phase portraits for the torso Euler angles and prosthetic hip angle in the frontal plane during 100 consecutive steps of the rigid simulator by the BMI optimized decentralized feedback control scheme. Convergence to the orbit is clear.

The flight phase model of the robot subject to these forces is then integrated as an ODE over time. This has several consequences. First, the evolution of the model subject to compliant ground reaction forces and non-instantaneous impact models can be addressed. Second, the robustness of the closed-loop system to different models of the ground is analyzed.

Figure 6 depicts the phase portraits of the closed-loop compliant model. Here the simulation starts from the initial condition of Fig. 4 and the system's solution converges to a *new stable* limit cycle. The animation of this simulation can be found at [66]. Unlike the phase portraits of the rigid simulator in Fig. 4, the new yaw and roll phase portraits of Fig. 6 are not symmetric with respect to the origin. In particular for the compliant model, the average yaw and roll angles for the steady-state walking motion become 5 (deg) and -1 (deg), respectively, which result in typical asymmetry in amputee locomotion. To describe this motion, we remark that the compliant dynamic model of the robot has left-right symmetry. However, the local controller structure of (10) and (11) does *not* have the left-right symmetry which may yield the left-right asymmetry in the presence of *nonparametric uncertainties*. In addition, the design of the orbit and optimized parameters were from the rigid simulator, i.e., no design of a new symmetric gait in the compliant model. Finally, we note that the robot's hip joints have only 2 DOFs, with rotations in the sagittal and frontal planes, but lack internal/external rotations in the transverse plane. One possible way to accommodate asymmetries in the torso yaw angle, arising from uncertainties, would then be to change the robot's morphology by having 3 DOFs hip joints to include yaw actuation.

E. Imposed Virtual Constraints for the Human Part

In Section VII-B, the iterative BMI algorithm optimized stabilizing local virtual constraints for the human and prosthetic
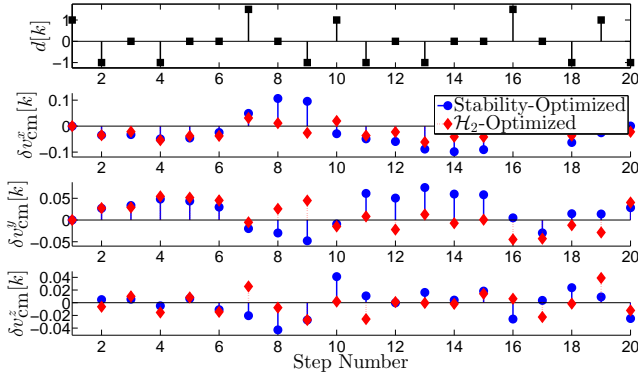
Fig. 5: Plot of an additive discrete-time disturbance $d[k]$ (deg/s) in the velocity components of the impact model and the corresponding x, y, and z components of the deviation in the robot's COM velocity ($\delta c[k] := \delta v_{cm}[k]$) on the Poincaré section to compare of the performances of the stability- and $\mathcal{H}_2$-optimized decentralized virtual constraints.

Fig. 6: Phase portraits for the torso Euler angles and prosthetic hip angle in the frontal plane during 100 consecutive steps of the compliant simulator by the BMI optimized decentralized feedback control scheme. Convergence to an orbit is clear.

leg parts simultaneously. The objective of the present section is to show that the proposed approach is still capable of finding a set of stabilizing virtual constraints for the prosthesis while using imposed virtual constraints for the human part that are known (e.g., through intuition or motion capture studies). In particular, we assume that the output matrix $H_1(\xi_1) \in \mathbb{R}^{3 \times 6}$ is known for the human part and the BMI algorithm only optimizes the prosthesis output matrices (i.e., $H_2(\xi_2) \in \mathbb{R}^{3 \times 3}$ and $\hat{H}_2(\xi_2) \in \mathbb{R}^{3 \times 4}$) to stabilize the walking gait. In this case, the total number of controller parameters to be determined is $(12 + 9) \times 2 = 42$ as we need to determine these matrices for the right and left stance phases. To simplify the example, the output matrix $H_1(\xi_1)$ for the human part is chosen intuitively.

Here we study two different scenarios. In the first scenario, we choose the controlled variables $H_1(\xi_1) q_1$ to control the shape variables for the human part. In particular, the components of $H_1(\xi_1) q_1$ are defined as the right knee and right two hip angles. For this choice of the H_1 matrix, the BMI algorithm could *not* converge to any stabilizing virtual constraints for the prosthesis. However for the second scenario, we let the human controlled variables $H_1(\xi_1) q_1$ have a feedback from the torso roll angle in the frontal plane. Then starting from the stabilizing solution obtained in Section VII-B, the algorithm successfully converges to a set of new stabilizing parameters for the prosthesis after 2 iterations. Figure 7 depicts the phase portraits for the torso Euler angles and frontal prosthetic hip angle during 100 consecutive walking steps. Convergence to the periodic orbit is clear. However compared to Fig. 4, the convergence rate is slower as only the prosthetic leg controller was optimized to stabilize the gait. These scenarios demonstrate how the most obvious choice for controlled variables (the shape variables) does not enable stability, which demonstrates the benefit of letting the BMI optimization algorithm determine this. However, one can still generate stable gaits when parts of the control system are fixed in a certain way.
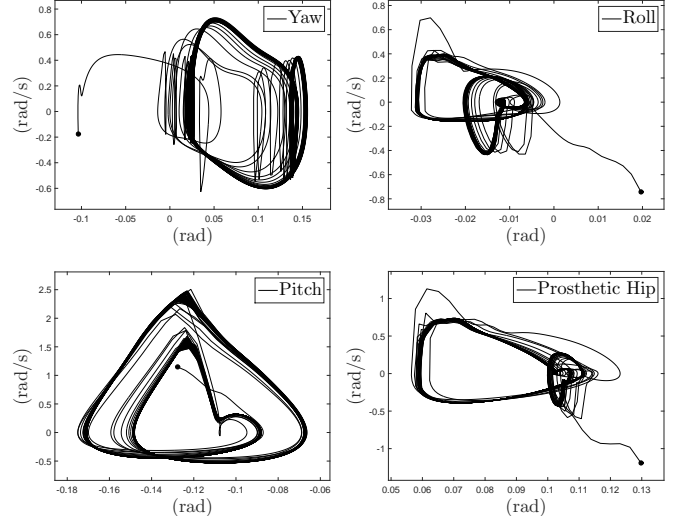
VIII. CONCLUSION

This paper introduced a systematic numerical algorithm for the design of decentralized feedback controllers to exponentially and robustly stabilize periodic orbits for hybrid dynamical systems arising from bipedal robots. The algorithm addresses the exponential and $\mathcal{H}_2$ robust stabilization problems of periodic orbits against uncertainties in discrete-time portions of hybrid models. We assumed a class of time-invariant, parameterized and local nonlinear controllers in which the coordination of lower-dimensional hybrid subsystems is done by a common and measurable phasing variable. It was also supposed that by employing this class of feedback laws, the periodic orbit is invariant under the choice of controller parameters. The algorithm then translated the exponential and $\mathcal{H}_2$ robust stabilization problems into an iterative sequence of optimization problems involving BMIs and LMIs. By design, these optimization problems can be solved with available software packages. Sufficient conditions for the convergence of the iterative algorithm to a robust stabilizing solution were presented. To illustrate the power of the algorithm, the paper employed the algorithm to systematically design a set of decentralized virtual constraints for walking of an underactuated 3D biped with 18 state variables and 78 controller parameters. The key features of the algorithm are as follows: (1) it considers a general form of parameterized nonlinear controllers; (2) the algorithm accounts for underactuation and impact model uncertainties; and (3) it deals with strong interactions among subsystems without relying on high-gain local controllers or expensive force sensors. For future research, we will investigate the scalability of the algorithm and its capability in stabilizing larger size interconnected systems for walking of quadruped robots. The current work considered discrete-time uncertainties, and future work will investigate robust stabilization of 3D walking gaits in the presence of a
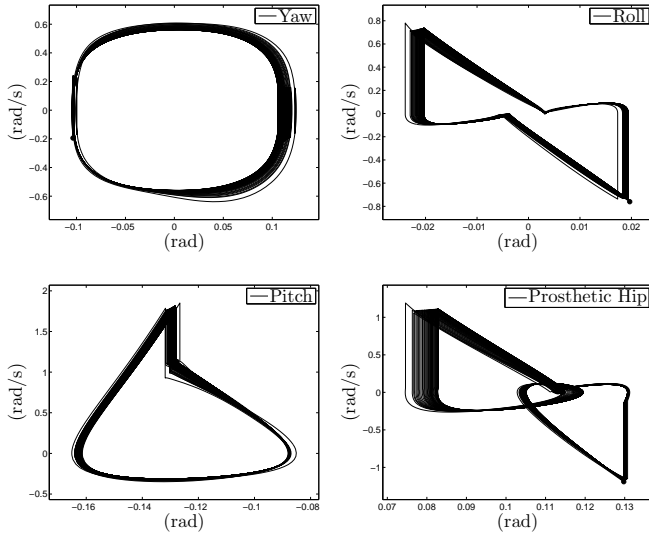
Fig. 7: Phase portraits for the torso Euler angles and prosthetic hip angle in the frontal plane during 100 consecutive steps. Here the BMI algorithm only optimized the virtual constraints for the prosthesis while the virtual constraints for the human part were imposed. Convergence to the periodic orbit $\mathcal{O}$ is clear.

broader range of model uncertainties including continuous and discrete-time uncertainties.

APPENDIX A
PROOF OF LEMMA 1

For every $\gamma > 0$ and any given square matrix A, $\rho(A) < \gamma$ is equivalent to $\rho(\frac{1}{\gamma}A) < 1$ which in turn is equivalent to the matrix $\frac{1}{\gamma}A$ being Hurwitz. From Lyapunov inequality, this is also equivalent to the existence of a positive definite matrix $Y = Y^\top$ such that $\frac{1}{\gamma^2}A^\top Y A - Y < 0$. Choosing $W = Y^{-1}$ and pre and post multiplying this latter inequality with W and applying Schur's complement lemma result in

$$\begin{bmatrix} W & A\,W \\ \star & \gamma^2\,W \end{bmatrix} > 0.$$

We remark that from the optimization problem (37)-(39), $\gamma < 1$. Using this fact, one can choose $\gamma^2 = 1 - \mu$ with $0 < \mu < 1$. This together with the LMI condition (27), guaranteeing $\eta > \|\Delta\xi\|_2^2$, completes the proof.

APPENDIX B
PROOF OF THEOREM 1

For the scalar case, $\rho(\hat{A}(\xi^\ell, \Delta\xi)) = |\hat{a}(\xi^\ell, \Delta\xi)| = |a^\ell + a'^\ell \Delta\xi|$, where $a^\ell := a(\xi^\ell)$ and $a'^\ell := a'(\xi^\ell)$. This reduces the equivalent optimization problem (37)-(39) to

$$\min_{\Delta\xi, \gamma} \frac{1}{2}\,w\,\gamma^2 + \frac{1}{2}\,\Delta\xi^2 \tag{46}$$

$$|a^\ell + a'^\ell \Delta\xi| = \gamma \tag{47}$$

$$\gamma < 1. \tag{48}$$

By assuming $a'^\ell \neq 0$ and $\frac{|a^\ell|}{w(a'^\ell)^2+1} < 1$ (see (40)), one can apply the Lagrange's multipliers approach to show that the global optimal solution of (46)-(48) is given by $\gamma^\star = \frac{a^\ell}{w(a'^\ell)^2+1}$ for $a^\ell \geq 0$ or $\gamma^\star = -\frac{a^\ell}{w(a'^\ell)^2+1}$ for $a^\ell < 0$. Furthermore, $\Delta\xi^\star$ becomes $\Delta\xi^\star = -\frac{w\,a^\ell\,a'^\ell}{w(a'^\ell)^2+1}$ which results in the parameter update law given in (41). It can also be shown that $\bar{\xi}$ is a fixed point for the parameter update law (41), i.e., $Q(\bar{\xi}) = \bar{\xi}$. This fact in combination with $a'(\xi) \neq 0$ for all $\xi \in \mathcal{B}$ implies that $0 < \frac{dQ}{d\xi}(\bar{\xi}) = \frac{1}{w(a'(\xi))^2+1} < 1$ which guarantees the local exponential stability of the fixed point $\bar{\xi}$. In particular, there exists $\delta > 0$ such that for all initial guesses $\xi^0 \in \mathcal{B}$ with the property $|\xi^0 - \bar{\xi}| < \delta$, $|\xi^\ell - \bar{\xi}| < \delta$, $\ell = 0, 1, \cdots$, and hence, $\xi^\ell \in \mathcal{B}$. This together with $a'(\xi) \neq 0$ for all $\xi \in \mathcal{B}$ and (40) validates our assumptions for extracting the global optimal solution of (46)-(48) at each iteration. Furthermore, $\lim_{\ell \to \infty} \xi^\ell = \bar{\xi}$. Finally, from the continuity of $a(.)$, one can conclude that $\lim_{\ell \to \infty} a(\xi^\ell) = a(\lim_{\ell \to \infty} \xi^\ell) = a(\bar{\xi}) = 0$ which in turn implies the existence of $0 < N < \infty$ such that $|a(\xi^\ell)| < 1$ for all $\ell > N$.

APPENDIX C
CONSTRUCTION PROCEDURE OF THE FUNCTION $F(a, \gamma)$

To construct the smooth function $F : \mathbb{R}^{n^2} \times \mathbb{R}_{>0} \to \mathbb{R}^{n+1}$, we apply the Jury stability criterion to the polynomial $\frac{1}{\gamma^n}\chi(\gamma z)$, and hence, the first two components of F are constructed as follows

$$F_1(a, \gamma) := -\frac{1}{\gamma^n}\chi(\gamma) = -\det\left(I - \frac{1}{\gamma}A\right)$$

$$F_2(a, \gamma) := (-1)^{n+1}\frac{1}{\gamma^n}\chi(-\gamma) = (-1)^{n+1}\det\left(-I - \frac{1}{\gamma}A\right).$$

The remaining $n - 1$ components of F are formed based on the Jury array. In particular from the Jury array, one can obtain a set of conditions as $|\underline{\kappa}_j(a, \gamma)| < |\overline{\kappa}_j(a, \gamma)|$ for $j = 1, \cdots, n - 1$. To make the function F smooth, the remaining $n - 1$ components of F can then be defined as

$$F_\alpha(a, \gamma) := \underline{\kappa}_{\alpha-2}^2(a, \gamma) - \overline{\kappa}_{\alpha-2}^2(a, \gamma) < 0$$

for $\alpha = 3, \cdots, n + 1$.

APPENDIX D
PROOF OF THEOREM 2

If the BMI optimization problem (25)-(28) is feasible during the iteration number ℓ, we can conclude that

$$F_\alpha\left(\hat{a}\left(\xi^\ell, \Delta\xi^\star\right), \gamma^\star\right) < 0, \quad \alpha = 1, \cdots, n + 1,$$

where $\gamma^\star := \sqrt{1 - \mu^\star}$. Now let us define the *error function* $E : \mathbb{R}^p \to \mathbb{R}^{n+1}$ by

$$E_\alpha(\Delta\xi) := F_\alpha\left(a\left(\xi^\ell + \Delta\xi\right), \gamma^\star\right) - F_\alpha\left(\hat{a}\left(\xi^\ell, \Delta\xi\right), \gamma^\star\right)$$

for every $\alpha = 1, \cdots, n + 1$. According to the construction procedure and the fact that $\hat{a}(\xi^\ell, \Delta\xi) = a(\xi^\ell) + \frac{\partial a}{\partial\xi}(\xi^\ell)\Delta\xi$,

$$\frac{\partial E_\alpha}{\partial \Delta\xi}(\Delta\xi) = \sum_{\beta=1}^{n^2} \frac{\partial F_\alpha}{\partial a_\beta}\left(a\left(\xi^\ell + \Delta\xi\right), \gamma^\star\right)\frac{\partial a_\beta}{\partial\xi}\left(\xi^\ell + \Delta\xi\right)$$

$$- \sum_{\beta=1}^{n^2} \frac{\partial F_\alpha}{\partial a_\beta}\left(\hat{a}\left(\xi^\ell, \Delta\xi\right), \gamma^\star\right)\frac{\partial a_\beta}{\partial\xi}\left(\xi^\ell\right).$$

This implies that $E_\alpha(0) = 0$ and $\frac{\partial E_\alpha}{\partial \Delta \xi}(0) = 0$ for $\alpha = 1, \cdots, n+1$. Straight forward calculations also result in

$$\frac{\partial^2 E_\alpha}{\partial \Delta \xi^2}(0) = \sum_{\beta=1}^{n^2} \frac{\partial F_\alpha}{\partial a_\beta}\left(a\left(\xi^\ell\right), \gamma^\star\right) \frac{\partial^2 a_\beta}{\partial \xi^2}\left(\xi^\ell\right)$$

which in combination with the condition (42) guarantees the negative semi-definiteness of the Hessian matrices $\frac{\partial^2 E_\alpha}{\partial \Delta \xi^2}(0)$. In particular, sufficient optimality conditions are satisfied for $\Delta \xi = 0$ being a local maximum for $E_\alpha(\Delta \xi)$, $\alpha = 1, \cdots, n+1$. Hence, there is $\epsilon > 0$ such that for all $\|\Delta \xi\| < \epsilon$, $E_\alpha(\Delta \xi) \leq E_\alpha(0) = 0$. If $\|\Delta \xi^\star\| < \epsilon$, this latter inequality implies that

$$F_\alpha\left(a\left(\xi^\ell + \Delta \xi^\star\right), \gamma^\star\right) \leq F_\alpha\left(\hat{a}\left(\xi^\ell, \Delta \xi^\star\right), \gamma^\star\right) < 0$$

for $\alpha = 1, \cdots, n+1$, or equivalently, $\rho(A(\xi^\ell + \Delta \xi^\star)) < \gamma^\star$. Finally, from the equivalent optimization problem (37)-(39), $\gamma^\star < 1$ which completes the proof of $A(\xi^\ell + \Delta \xi^\star)$ being a Hurwitz matrix.

APPENDIX E
PROOF OF THEOREM 3

The proof is similar to that presented for Theorem 2 in Appendix D. We only need to extend the smooth function $F(a, \gamma)$ as proposed in the following lemma.

Lemma 2: For a given quadruple $(A, B, C, 0)$ with the matrices $A \in \mathbb{R}^{n \times n}$ and $B \in \mathbb{R}^{n \times n}$, there is a smooth function $\bar{F} : \mathbb{R}^{n^2} \times \mathbb{R}^{n^2} \times \mathbb{R}_{>0} \to \mathbb{R}^{n+2}$ such that

$$\bar{F}_\alpha(a, b, \mu) < 0, \quad \alpha = 1, \cdots, n+2 \qquad (49)$$

is equivalent to 1. the matrix A being Hurwitz, and 2. the $\mathcal{H}_2$-norm of the transfer function corresponding to the quadruple $(A, B, C, 0)$ becomes less than $\sqrt{\mu}$.

Proof: From Appendix C, the matrix A being Hurwitz is equivalent to $F(a, 1) < 0$. For a Hurwitz matrix A, it is well-known that the $\mathcal{H}_2$-norm of the transfer function corresponding to the quadruple $(A, B, C, 0)$ can be computed numerically as follows

$$\|T_{dc}(z)\|_{\mathcal{H}_2}^2 = \text{trace}\left(B^\top W_o B\right), \qquad (50)$$

where W_o is the observability Gramian satisfying the Lyapunov equation $A^\top W_o A - W_o = -C^\top C$. Consequently, one can define the smooth scalar function $\tilde{F}(a, b, \mu) := \text{trace}\left(B^\top W_o B\right) - \mu$ such that $\tilde{F}(a, b, \mu) < 0$ is equivalent to $\|T_{dc}(z)\|_{\mathcal{H}_2}^2 < \mu$. Finally, $\bar{F}(a, b, \mu)$ can be constructed as follows

$$\bar{F}(a, b, \mu) := \begin{bmatrix} F(a, 1) \\ \tilde{F}(a, b, \mu) \end{bmatrix} \in \mathbb{R}^{n+2}. \qquad (51)$$

$\blacksquare$

The proof of Theorem 3 can be completed by defining an error function as

$$E(\Delta \xi) := \bar{F}\left(a\left(\xi^\ell + \Delta \xi\right), b\left(\xi^\ell + \Delta \xi\right), \mu^\star\right)$$
$$- \bar{F}\left(\hat{a}\left(\xi^\ell, \Delta \xi\right), \hat{b}\left(\xi^\ell, \Delta \xi\right), \mu^\star\right)$$

and following the steps of Appendix D and Remark 6.

REFERENCES

[1] G. Song and M. Zefran, "Underactuated dynamic three-dimensional bipedal walking," in *Robotics and Automation. Proceedings IEEE International Conference on*, May 2006, pp. 854–859.

[2] J. Grizzle, G. Abba, and F. Plestan, "Asymptotically stable walking for biped robots: analysis via systems with impulse effects," *Automatic Control, IEEE Transactions on*, vol. 46, no. 1, pp. 51–64, Jan 2001.

[3] E. Westervelt, J. Grizzle, and D. Koditschek, "Hybrid zero dynamics of planar biped walkers," *Automatic Control, IEEE Transactions on*, vol. 48, no. 1, pp. 42–56, Jan 2003.

[4] E. Westervelt, J. Grizzle, C. Chevallereau, J. Choi, and B. Morris, *Feedback Control of Dynamic Bipedal Robot Locomotion*. Taylor & Francis/CRC, 2007.

[5] K. Akbari Hamed and J. Grizzle, "Event-based stabilization of periodic orbits for underactuated 3-D bipedal robots with left-right symmetry," *Robotics, IEEE Transactions on*, vol. 30, no. 2, pp. 365–381, April 2014.

[6] M. Spong and F. Bullo, "Controlled symmetries and passive walking," *Automatic Control, IEEE Transactions on*, vol. 50, no. 7, pp. 1025–1031, July 2005.

[7] M. Spong, J. Holm, and D. Lee, "Passivity-based control of bipedal locomotion," *Robotics Automation Magazine, IEEE*, vol. 14, no. 2, pp. 30–40, June 2007.

[8] R. Gregg and L. Righetti, "Controlled reduction with unactuated cyclic variables: Application to 3D bipedal walking with passive yaw rotation," *Automatic Control, IEEE Transactions on*, vol. 58, no. 10, pp. 2679–2685, Oct 2013.

[9] R. Gregg, A. Tilton, S. Candido, T. Bretl, and M. Spong, "Control and planning of 3-D dynamic walking with asymptotically stable gait primitives," *Robotics, IEEE Transactions on*, vol. 28, no. 6, pp. 1415–1423, Dec 2012.

[10] A. Ames, R. Gregg, and M. Spong, "A geometric approach to three-dimensional hipped bipedal robotic walking," in *Decision and Control, 46th IEEE Conference on*, Dec 2007, pp. 5123–5130.

[11] A. Ames, "Human-inspired control of bipedal walking robots," *Automatic Control, IEEE Transactions on*, vol. 59, no. 5, pp. 1115–1130, May 2014.

[12] A. Ames, K. Galloway, K. Sreenath, and J. Grizzle, "Rapidly exponentially stabilizing control Lyapunov functions and hybrid zero dynamics," *Automatic Control, IEEE Transactions on*, vol. 59, no. 4, pp. 876–891, April 2014.

[13] C. Chevallereau, J. Grizzle, and C.-L. Shih, "Asymptotically Stable Walking of a Five-Link Underactuated 3-D Bipedal Robot," *Robotics, IEEE Transactions on*, vol. 25, no. 1, pp. 37–50, Feb 2009.

[14] A. Ramezani, J. Hurst, K. Akbai Hamed, and J. Grizzle, "Performance analysis and feedback control of ATRIAS, a three-dimensional bipedal robot," *Journal of Dynamic Systems, Measurement, and Control December, ASME*, vol. 136, no. 2, December 2013.

[15] H. Dai and R. Tedrake, "$\mathcal{L}_2$-gain optimization for robust bipedal walking on unknown terrain," in *Robotics and Automation, IEEE International Conference on*, May 2013, pp. 3116–3123.

[16] I. R. Manchester, U. Mettin, F. Iida, and R. Tedrake, "Stable dynamic walking over uneven terrain," *The International Journal of Robotics Research*, vol. 30, no. 3, pp. 265–279, 2011.

[17] J. Pratt, T. Koolen, T. de Boer, J. Rebula, S. Cotton, J. Carff, M. Johnson, and P. Neuhaus, "Capturability-based analysis and control of legged locomotion, part 2: Application to M2V2, a lower-body humanoid," *The International Journal of Robotics Research*, vol. 31, no. 10, pp. 1117–1133, 2012.

[18] K. Byl and R. Tedrake, "Approximate optimal control of the compass gait on rough terrain," in *Robotics and Automation. IEEE International Conference on*, May 2008, pp. 1258–1263.

[19] C. Saglam and K. Byl, "Switching policies for metastable walking," in *Decision and Control, IEEE 52nd Annual Conference on*, Dec 2013, pp. 977–983.

[20] A. D. Ames, R. W. Sinnet, and E. D. Wendel, "Three-dimensional kneed bipedal walking: A hybrid geometric approach," in *Hybrid Systems: Computation and Control*, ser. Lecture Notes in Computer Science, R. Majumdar and P. Tabuada, Eds. Springer Berlin Heidelberg, 2009, vol. 5469, pp. 16–30.

[21] C. D. Remy, "Optimal exploitation of natural dynamics in legged locomotion," Ph.D. dissertation, ETH Zurich, 2011.

[22] M. H. Raibert, "Legged robots," *Communications of the ACM*, vol. 29, no. 6, p. 499514, 1986.

[23] M. Donner, *Real-Time Control of Walking*. Birkhäuser Boston, 1987.

[24] M. Eilenberg, H. Geyer, and H. Herr, "Control of a powered ankle–foot prosthesis based on a neuromuscular model," *IEEE Transactions on Neural Systems and Rehabilitation Engineering*, vol. 18, no. 2, pp. 164–173, 2010.

[25] Össur. POWER KNEE. http://www.ossur.com/powerknee/. [Online]. Available: http://www.ossur.com/powerknee/

[26] F. Sup, H. Varol, and M. Goldfarb, "Upslope walking with a powered knee and ankle prosthesis: Initial results with an amputee subject," *IEEE Transactions on Neural Systems and Rehabilitation Engineering*, vol. 19, no. 1, pp. 71–78, 2011.

[27] A. M. Simon, K. A. Ingraham, N. P. Fey, S. B. Finucane, R. D. Lipschutz, A. J. Young, and L. J. Hargrove, "Configuring a powered knee and ankle prosthesis for transfemoral amputees within five specific ambulation modes," *PloS ONE*, vol. 9, no. 6, p. e99387, 2014.

[28] R. Gregg, T. Lenzi, L. Hargrove, and J. Sensinger, "Virtual constraint control of a powered prosthetic leg: From simulation to experiments with transfemoral amputees," *Robotics, IEEE Transactions on*, vol. 30, no. 6, pp. 1455–1471, Dec 2014.

[29] R. Gregg and J. Sensinger, "Towards biomimetic virtual constraint control of a powered prosthetic leg," *Control Systems Technology, IEEE Transactions on*, vol. 22, no. 1, pp. 246–254, Jan 2014.

[30] A. Martin and R. Gregg, "Hybrid invariance and stability of a feedback linearizing controller for powered prostheses," in *American Control Conference*, 2015, pp. 4670–4676.

[31] L. Bakule, "Decentralized control: An overview," *Annual Reviews in Control*, vol. 32, no. 1, pp. 87–98, 2008.

[32] S.-H. Wang and E. Davison, "On the stabilization of decentralized control systems," *Automatic Control, IEEE Transactions on*, vol. 18, no. 5, pp. 473–478, Oct 1973.

[33] D. Siljak, *Decentralized Control of Complex Systems*. Dover Publications, December 2011.

[34] W. Haddad, V. Chellaboina, and S. Nersesov, *Impulsive and Hybrid Dynamical Systems: Stability, Dissipativity, and Control*. Princeton University Press, July 2006.

[35] R. Goebel, R. Sanfelice, and A. Teel, *Hybrid Dynamical Systems: Modeling, Stability, and Robustness*. Princeton University Press, March 2012.

[36] D. Bainov and P. Simeonov, *Systems With Impulse Effect: Stability, Theory and Applications*. Ellis Horwood Ltd, June 1989.

[37] H. Ye, A. Michel, and L. Hou, "Stability theory for hybrid dynamical systems," *Automatic Control, IEEE Transactions on*, vol. 43, no. 4, pp. 461–474, Apr 1998.

[38] T. Parker and L. Chua, *Practical Numerical Algorithms for Chaotic Systems*. Springer, 1989.

[39] S. Burden, S. Revzen, and S. Sastry, "Model reduction near periodic orbits of hybrid dynamical systems," *Automatic Control, IEEE Transactions on*, vol. to appear, 2015.

[40] W. Haddad and V. Chellaboina, *Nonlinear Dynamical Systems and Control: A Lyapunov-Based Approach*. Princeton University Press, February 2008.

[41] K. Akbari Hamed, B. Buss, and J. Grizzle, "Exponentially stabilizing continuous-time controllers for periodic orbits of hybrid systems: Application to bipedal locomotion with ground height variations," *The International Journal of Robotics Research*, August 2015, [Published Online, DOI: 10.1177/0278364915593400].

[42] ——, "Continuous-time controllers for stabilizing periodic orbits of hybrid systems: Application to an underactuated 3D bipedal robot," in *Decision and Control (CDC), 2014 IEEE 53rd Annual Conference on*, Dec 2014, pp. 1507–1513.

[43] K. Akbari Hamed and J. Grizzle, "Iterative robust stabilization algorithm for periodic orbits of hybrid dynamical systems: Application to bipedal running," in *The IFAC Conference on Analysis and Design of Hybrid Systems*, June 2015, accepted to appear. [Online]. Available: {http://www-rohan.sdsu.edu/%7Ekavehah/IFAC%5F2015.pdf}

[44] B. G. Buss, K. Akbari Hamed, B. A. Griffin, and J. W. Grizzle, "Experimental results for 3D bipedal robot walking based on systematic optimization of virtual constraints," in *The 2016 American Control Conference*, July 2016, accepted to appear. [Online]. Available: {http://web.eecs.umich.edu/%7Egrizzle/papers/ACC2016%5FBussAkbariHamedGriffinGrizzle.pdf}

[45] Dynamic Leg Locomotion YouTube Channel. (2015) MARLO: Dynamic 3D walking based on HZD gait design and BMI constraint selection. [Online]. Available: https://www.youtube.com/watch?v=5ms5DtPNwHo

[46] K. Akbari Hamed and R. D. Gregg, "Decentralized feedback controllers for exponential stabilization of hybrid periodic orbits: Application to robotic walking," in *The 2016 American Control Conference*, July

[47] H. Zhao, J. Horn, J. Reher, V. Paredes, and A. D. Ames, "A hybrid systems and optimization-based control approach to realizing multi-contact locomotion on transfemoral prostheses," in *54th IEEE Conference on Decision and Control*, Osaka, Japan, 2015.

2016, accepted to appear. [Online]. Available: {http://www-rohan.sdsu.edu/%7Ekavehah/Decentralized%5FACC2016.pdf}

[48] W. Flowers and R. Mann, "Electrohydraulic knee-torque controller for a prosthesis simulator," *ASME J. of Biomechanical Engineering*, vol. 99, no. 4, pp. 3–8, 1977.

[49] D. J. Villarreal, H. Poonawala, and R. D. Gregg, "A robust parameterization of human gait patterns across phase-shifting perturbations," *IEEE Transactions Neural Systems and Rehabilitation Engineering*, 2015, under review.

[50] J. W. Grizzle, C. Chevallereau, R. W. Sinnet, and A. D. Ames, "Models, feedback control, and open problems of 3D bipedal robotic walking," *Automatica*, vol. 50, no. 8, pp. 1955–1988, 2014.

[51] A. Isidori, *Nonlinear Control Systems*. Springer; 3rd edition, 1995.

[52] C. De Oliveira, J. Geromel, and J. Bernussou, "Extended $\mathcal{H}_2$ and $\mathcal{H}_\infty$ norm characterizations and controller parametrizations for discrete-time systems," *International Journal of Control*, vol. 75, no. 9, pp. 666–679, 2002.

[53] J. Lack, M. Powell, and A. Ames, "Planar multi-contact bipedal walking using hybrid zero dynamics," in *Robotics and Automation, IEEE International Conference on*, May 2014, pp. 2582–2588.

[54] C. Chevallereau, G. Abba, Y. Aoustin, F. Plestan, E. Westervelt, C. Canudas-de Wit, and J. Grizzle, "RABBIT: a testbed for advanced control theory," *Control Systems Magazine, IEEE*, vol. 23, no. 5, pp. 57–79, Oct 2003.

[55] K. Sreenath, H.-W. Park, I. Poulakakis, and J. Grizzle, "Embedding active force control within the compliant hybrid zero dynamics to achieve stable, fast running on mabel," vol. 32, no. 3, pp. 324–345, 2013.

[56] M. Maggiore and L. Consolini, "Virtual holonomic constraints for Euler Lagrange systems," *Automatic Control, IEEE Transactions on*, vol. 58, no. 4, pp. 1001–1008, April 2013.

[57] A. Shiriaev, A. Sandberg, and C. Canudas de Wit, "Motion planning and feedback stabilization of periodic orbits for an acrobot," in *Decision and Control. 43rd IEEE Conference on*, vol. 1, Dec 2004, pp. 290–295 Vol.1.

[58] A. E. Martin, D. C. Post, and J. P. Schmiedeler, "The effects of foot geometric properties on the gait of planar bipeds walking under HZD-based control," vol. 33, no. 12, pp. 1530–1543, 2014.

[59] P. de Leva, "Adjustments to Zatsiorsky-Seluyanov's segment inertia parameters," *J Biomech*, vol. 29, no. 9, pp. 123–1230, 1996.

[60] Y. Hurmuzlu and D. B. Marghitu, "Rigid body collisions of planar kinematic chains with multiple contact points," vol. 13, no. 1, pp. 82–92, 1994.

[61] Wikipedia. (2014) Computational complexity of mathematical operations, http://en.wikipedia.org/wiki/Computational_complexity_of_mathematical_operations. [Online]. Available: http://en.wikipedia.org/wiki/Computational_complexity_of_mathematical_operations

[62] O. Toker and H. Ozbay, "On the NP-hardness of solving bilinear matrix inequalities and simultaneous stabilization with static output feedback," in *American Control Conference, Proceedings of the 1995*, vol. 4, Jun 1995, pp. 2525–2526 vol.4.

[63] D. Henrion, J. Lofberg, M. Kocvara, and M. Stingl, "Solving polynomial static output feedback problems with PENBMI," in *Decision and Control, and European Control Conference. 44th IEEE Conference on*, Dec 2005, pp. 7581–7586.

[64] TOMLAB optimization, http://tomopt.com/tomlab/.

[65] J. Lofberg, "YALMIP : a toolbox for modeling and optimization in MATLAB," in *Computer Aided Control Systems Design, 2004 IEEE International Symposium on*, Sept 2004, pp. 284–289.

[66] K. Akbari Hamed YouTube Channel. (2015) Decentralized feedback controllers for robust stabilization of periodic orbits of hybrid systems, https://www.youtube.com/watch?v=VwUARpR0hKk&feature=youtu.be.

[67] F. Plestan, J. Grizzle, E. Westervelt, and G. Abba, "Stable walking of a 7-DOF biped robot," *Robotics and Automation, IEEE Transactions on*, vol. 19, no. 4, pp. 653–668, Aug 2003.

[68] C. De Wit, H. Olsson, K. Astrom, and P. Lischinsky, "A new model for control of systems with friction," *Automatic Control, IEEE Transactions on*, vol. 40, no. 3, pp. 419–425, Mar 1995.

Kaveh Akbari Hamed (M'15) received the B.S. degree in electrical engineering from the University of Tabriz in 2004 and the M.S. and Ph.D. degrees in electrical engineering (Control Engineering) from the Sharif University of Technology, Tehran, Iran in 2006 and 2011, respectively.

He is currently an assistant professor in Mechanical Engineering at San Diego State University. Before joining San Diego State University, he was a postdoctoral research fellow working at the Department of Electrical Engineering and Computer Science of the University of Michigan from 2012 to 2014. His research interests include nonlinear and robust control, robotics, dynamical legged locomotion, hybrid systems, and optimization.

Robert D. Gregg IV (S'08-M'10-SM'16) received the B.S. degree (2006) in electrical engineering and computer sciences from the University of California, Berkeley and the M.S. (2007) and Ph.D. (2010) degrees in electrical and computer engineering from the University of Illinois at Urbana-Champaign.

He joined the Departments of Bioengineering and Mechanical Engineering at the University of Texas at Dallas as an Assistant Professor in June 2013. Prior to joining UT Dallas, he was a Research Scientist at the Rehabilitation Institute of Chicago and a Postdoctoral Fellow at Northwestern University. His research is in the control of bipedal locomotion with applications to autonomous and wearable robots.